https://doi.org/10.5194/egusphere-2023-42
Preprint. Discussion started: 26 January 2023
© Author(s) 2023. CC BY 4.0 License.

A new high-resolution Coastal Ice-Ocean Prediction System for the East Coast of Canada

Jean-Philippe Paquin[1], François Roy[1], Gregory C. Smith[1], Sarah MacDermid[2,4], Ji Lei[2,3], Frédéric Dupont[2], Youyu Lu[4], Stephanne Taylor[4], Simon St-Onge-Drouin[5], Hauke Blanken[6], Michael Dunphy[6], Nancy Soontiens[7]

[1] Division de la Recherche en Météorologie, Environnement et changement climatique Canada, Dorval, Canada

[2] Service Météorologique du Canada, Environnement et changement climatique Canada, Dorval, Canada

[3] Canadian Hydrographic Services, Fisheries and Oceans Canada, Dorval, Canada

[4] Bedford Institute of Oceanography, Fisheries and Oceans Canada, Dartmouth, Canada

[5] Institut Maurice-Lamontagne, Pêches et Océans Canada, Mont Joli, Canada

[6] Institute of Ocean Sciences, Fisheries and Oceans Canada, Victoria, Canada

[7] North Atlantic Fisheries Centre, Fisheries and Oceans Canada, St. John's, Canada

Correspondence to: Jean-Philippe Paquin (jean-philippe.paquin@ec.gc.ca)

© 2023 His Majesty the King in Right of Canada. Reproduced with thte permission of the Minister of Environment and climate change Canada

Abstract.

This paper describes the Coastal Ice Ocean Prediction System for the East Coast of Canada (CIOPS-E) running operationally at Environment and Climate Change Canada (ECCC). CIOPS-E uses a one-way downscaling technique on a 1/36° horizontal grid (~2 km) to simulate high-resolution ice and ocean conditions over the northwest Atlantic Ocean and the Gulf of St. Lawrence (GSL). CIOPS-E is forced at its lateral boundaries with ECCC's Regional Ice-Ocean Prediction System (RIOPS) and tidal conditions from the Oregon State University TPXO model. The three-dimensional temperature and salinity fields are spectrally nudged towards the RIOPS solution offshore of the 1500 m isobath to, effectively constrain mesoscale features in the Gulf Stream area. Over the continental shelf and the GSL, the CIOPS-E solution is free to develop fully according to model dynamics.

CIOPS-E is evaluated over one year from March 2019 to February 2020. Overall, the CIOPS-E improves the representation of tides compared to ECCC's lower resolution systems: RIOPS (1/12°) and the Regional Marine Prediction System – Gulf of St. Lawrence (RMPS-GSL, 5 km). The accuracy of the tides are comparable to the TPXO at most coastal tide gauges. Sub-tidal water levels from CIOPS-E agree well with the observed seasonal variability and show improved errors statistics at all stations compared to RIOPS and RMPS-GSL. Improvements are especially noted for the GSL.

Sea surface temperatures (SSTs) from CIOPS-E are lower (higher) in spring (fall) over most of the GSL compared to satellite-derived analyses and RIOPS. Comparison with in-situ observations of SST show significant improvement in CIOPS-E with

https://doi.org/10.5194/egusphere-2023-42
Preprint. Discussion started: 26 January 2023
© Author(s) 2023. CC BY 4.0 License.

respect to the RMPS-GSL. Lastly, sea ice conditions in the GSL are compared with the Canadian Ice Service (CIS) charts and the RMPS-GSL model. The sea ice cover and thickness from the pseudo-analysis component (without data assimilation) shows an overestimation compared to the CIS estimates, which is subsequently corrected in the forecast phase through the direct insertion of a Radarsat image analysis product.

1. Introduction

This paper describes the new Coastal Ice-Ocean Prediction System for the East Coast of Canada (CIOPS-E) developed and implemented operationally in 2021 at the Canadian Centre for Meteorological and Environmental Prediction (CCMEP, formerly the Canadian Meteorological Centre [CMC]), under the Government of Canada's Oceans Protection Plan (OPP) initiative. This high-resolution ice-ocean prediction system is developed with the objectives of (i) increasing the numerical guidance available in the eventuality of environmental emergencies in the aquatic environment and (ii) providing improved forecasting of water levels and near-surface currents to improve navigational safety.

Development of the CIOPS-E system is aligned with the world-wide increase in the number of ocean forecasting systems in coastal areas in recent years using horizontal resolutions in the order of a few kilometers. Examples of such systems include the Copernicus Marine System (CMS) Iberia-Biscay-Ireland regional modeling system (IBI; Maraldi et al. 2013; Lorente et al. 2019; Garcia Sotillo et al. 2021), the Western Mediterranean Operational System (WMOP; Aguiar et al. 2020) and the US West Coast Ocean Forecast System (WCOFS; Kurapov et al. 2017). Some ocean systems already have versions including data assimilation, such as the Met Office North-West European Shelf forecasting system (Tonani et al. 2029). Sakamoto et al. (2019) and Hirose et al. (2019) developed a data assimilative and operational forecasting model for the coastal and open-ocean areas around Japan. A coastal downscaling system for the Mediterranean Sea has been developed by combining structured and unstructured ocean models (Trotta et al. 2016, Trotta et al. 2017). The variety of systems developed and implemented world-wide also allows for different groups to improve our understanding of model behaviour and limitations via inter-model comparison studies (e.g., Nudds et al. 2020).

Horizontal grid resolution of a few kilometers is necessary to capture with some degrees of accuracy the complex coastal interactions over a broad range of spatial and temporal scales between near-shore dynamics, land hydrology and river discharge, and atmospheric forcing (Kourafalou et al. 2015a, b). Over the GSL, seasonal sea ice formation, dynamics and melt add to the complexity of interactions. As noted by De Mey-Frémaux et al. (2019), the development of high-resolution ocean-sea ice models used in a complementary approach with the observations and monitoring programs would also help improve the understanding of the coastal marine environment.

As part of the OPP oceanography sub-initiative, two high-resolution Coastal Ice-Ocean Predictions Systems (CIOPS) were developed covering the Atlantic and Pacific Coasts of Canada. The 1/36° (~2 km) resolution CIOPS systems are used to perform a dynamical downscaling of the operational 1/12° Region Ice-Ocean Prediction System (RIOPS; Smith et al. 2021) over the two environmentally sensitive and high density maritime transport areas of the country. The development of these

https://doi.org/10.5194/egusphere-2023-42
Preprint. Discussion started: 26 January 2023
© Author(s) 2023. CC BY 4.0 License.

high resolution coastal systems includes the refinements in the bathymetry and representation of coastlines combined with the use of higher resolution atmospheric forcing. This allows more realistic representation of the variations of current structures, and tidal and sub-tidal elevations at the coastal scales.

In addition to the direct contribution to environmental emergency response, CIOPS also directly supports sub-kilometer port-scale numerical models currently developed by the Canadian Department of Fisheries and Oceans (DFO), by providing high-resolution and high-frequency open ocean boundary conditions. The six port models currently in development are Saint John Harbour (Paquin et al. 2019), Canso and St. Lawrence Estuary on the east coast, and Kitimat, Vancouver Harbour and Fraser River on the west coast.

CIOPS-E has a pseudo-analysis and a forecast component. In the following sections, both components are evaluated and compared to current operational systems (RIOPS and RMPS-GSL). The evaluation is focused on variables influencing the representation of near-surface currents and water mass properties crucial to the emergency response capabilities: (i) tidal amplitudes and phases, (ii) sub-tidal water levels, (iii) sea surface temperatures, (iv) vertical profiles of temperature and salinity and (v) sea ice cover and thickness. The evaluations are presented in Section 4, after the introduction of CCMEP products used in evaluation (Section 2) and the details of the CIOPS-E ice-ocean modeling system components and experimental setup (Section 3). This is followed by a discussion of the system's limitations and future improvements and main conclusions in Section 5.

2. Description of other CCMEP products

First, we begin by describing other CCMEP (previously known as the Canadian Meteorological Centre, CMC) products used by CIOPS-E for boundary conditions and spectral nudging (see Section 3) as well as for the evaluation of CIOPS-E presented here. These include the CCMEP sea surface temperature analysis as well as the RIOPS and RMPS-GSL systems.

2.1 CCMEP sea surface temperature analysis

The CCMEP sea surface temperature analysis is a daily satellite-derived gridded product on a 0.1° resolution grid produced using an optimal interpolation (OI) methodology (Brasnett 2008, Brasnett and Surcel-Colan 2016).

2.2 Regional Ice-Ocean Prediction Systems

RIOPS is an ice-ocean prediction system covering all Canadian waters at a 1/12° grid resolution (Smith et al. 2021). RIOPS uses a similar ice-ocean configuration model to CIOPS. RIOPS produces daily analyses and 48 h forecasts on a 1/12° Pan-Canadian grid covering the Atlantic from 26°N, the Arctic Ocean and extends to 44°N in the Pacific Ocean. The ocean is initialized using a multi-variate reduced-order Kalman filter that assimilates satellite altimetry, temperature and salinity profiles (e.g., from Argo, field campaigns, moorings, drifting buoys, gliders, etc.). A 3DVar approach is used to provide a large-scale low-frequency correction to water mass properties based on innovations from profile observations. The ocean

https://doi.org/10.5194/egusphere-2023-42
Preprint. Discussion started: 26 January 2023
© Author(s) 2023. CC BY 4.0 License.

analysis is blended with a 3DVar sea ice analysis (Buehner et al., 2013; 2016) that incorporates satellite retrievals from various sources along with charts and Radarsat2 image analyses from the Canadian Ice Service. RIOPS has been shown to provide an adequate constraint on mesoscale features in the Gulf Stream region (Smith et al., 2021).

2.3 Regional Marine Prediction System for the Gulf of St. Lawrence

The Regional Marine Prediction System for the Gulf of St. Lawrence (RMPS-GSL; Roy et al. 2014; Smith et al. 2013; Pellerin et al. 2004) is a coupled atmosphere-ocean-sea ice prediction system that was providing daily ocean pseudo-analyses as well as four coupled 48h forecasts (executed at 00Z, 06Z, 12Z and 18Z). The Global Environmental Multiscale model (GEM; Bélair et al., 2000) with a 10 km resolution is used to provide forcing for the ice-ocean model during the pseudo-analysis phase, and is used to produce the fully coupled forecasts. The ice-ocean model is based on the Nucleus for European Modelling of the Ocean (NEMO) version 3.6 (Madec, 2015) coupled to the Los Alamos Community Ice CodE version 4 (CICEv4; Hunke 2001; Lipscomb et al., 2007; Hunke and Lipscomb, 2008). The ocean-sea ice model uses a rotated grid at a 5 km horizontal resolution, with climatological boundary conditions for temperature and salinity at Belle Isle and Cabot Straits. A 1-dimensional model of the St. Lawrence River (Lefaivre et al. 2016) is used to provide daily runoff estimates to an internal, 2-way coupling 1-D model that propagates the tide upstream, avoiding tidal reflection. The CIOPS-E model is adopted by the Water Cycle Prediction System as the ocean component, in addition to a separate 1-km NEMO configuration for the Great Lakes. With the development of the WCPS, the RMPS-GSL system was since decommissioned.

3. CIOPS-E System description

3.1 Ocean model

3.1.1 NEMO

The ocean component of CIOPS-E, NEMO version 3.6, solves the three-dimensional governing equations of ocean circulation and hydrography (temperature and salinity) on a structured computational grid. The governing equations include the hydrostatic and Boussinesq approximation. The ocean model uses 100 vertical z-levels, with spacing increasing from 1 m at the surface over the first 10 m, to 200 m at 5000 m depth. Bottom partial steps are employed for an accurate representation of the varying bathymetry. Further, the use of ‘‘variable volume level’’ (Levier et al. 2007) allows the thickness of the vertical levels to vary with changes in sea surface elevation.

The momentum advection follows the 3rd order Upstream-Biased Scheme (UBS; Shchepetkin and McWilliams, 2005). Along the lateral solid boundaries (coastline), a partial slip boundary condition is used to allow the frictional effects of the lateral boundaries to be included without the restrictive resolution required to represent the lateral boundary layer under no slip conditions. Tracers are advected using the Total Variance Dissipation (TVD) scheme in both horizontal and vertical directions (Madec et al., 2015). A vertical split-explicit time stepping with five sub-timesteps is used to ensure stability. The lateral

https://doi.org/10.5194/egusphere-2023-42
Preprint. Discussion started: 26 January 2023
© Author(s) 2023. CC BY 4.0 License.

diffusion on tracers and momentum uses 3D time-varying viscosity following Smagorinski (1993) where the viscosity coefficient is proportional to a local deformation rate based on horizontal shear and tension. A time-splitting scheme is applied for the internal (baroclinic) and external (barotropic) modes. The time step for the internal (external) mode is set to 150 s (5 s). Vertical turbulence and mixing are calculated through the k − ε configuration of the generic length scale (GLS) turbulence closure (Umlauf and Burchard 2003) with background vertical eddy viscosity and diffusivity set to 1.0×10^{-4} m^2 s^{-1} and 1.0×10^{-5} m^2 s^{-1}, respectively. Sensitivity experiments showed optimized tides in the St. Lawrence Estuary when using bottom non-linear log-layer formulation with bottom roughness of $2x10^{-4}$ m (Paquin et al. 2021, 2022). Table 1 summarizes the comparison of the main ocean model parameters between CIOPS-E and RIOPS.

Preliminary experiments revealed a large-scale cold surface bias in summer that was reduced through adjustments to the model's physics. First, the surface turbulent kinetic energy (TKE) input from wave breaking, where the significant wave height (H_s) is based on the Rascle et al. (2008) formula, was reduced by adjusting the multiplication factor used to compute the surface roughness length (z_0). A reduction of the roughness length (from $z_0 = 1.3H_s$ to $z_0 = 0.75H_s$) reduced the surface mixing in summer and hence the cold bias. A second adjustment to the ocean surface momentum transfer was included to 1) add a surface wave representation in the wind stress computation (expected to be more realistic in fall and winter) and 2) to make the wind stress computation consistent with the TKE wave breaking input formulas as noted above. The wave breaking TKE input formulas are based on Rascle et al. (2008) and Mellor and Blumberg (2004) where the relation between sea surface height (roughness) and wind stress is derived from Smith *et al.* (1992). Therein, the sea surface roughness length (z_{0a}) is derived from the following Charnock-type formula:

$$z_{0a} = \alpha \left(\frac{C_p}{u_*}\right)^{\beta} \frac{u_*^2}{g} \quad (1)$$

where Cp/u* is the wave age, u* is the friction velocity, g is the acceleration due to gravitation,and α=0.45 and β=-1 are tuneable parameters. Using this same formula instead of the one from Large and Yeager (2004) for the Common Ocean-ice Reference Experiments (CORE) makes the surface wind stress consistent with the TKE wave breaking input formula. The consequence is to have more surface mixing in fall and winter but slightly less in summer (for winds below 5 m s^{-1}). Finally, increased vertical mixing in the upper St. Lawrence Estuary is introduced to stimulate the estuarine circulation as the model resolution is not sufficient to resolve the mixing processes there related to the interaction of the large runoff from the St. Lawrence River with rugged topography and strong tides (Saucier and Chassé, 2000). We artificially increased the surface wind stress by 50% and vertical mixing coefficients (increase of $2x10^{-2}$ m^2 s^{-1}) west of Tadoussac (see Fig. 1). Impact studies for individual changes are presented in Paquin et al. (2021).

3.1.2 Model domain and bathymetry

CIOPS-E model domain (Fig. 1) follows the ORCA tri-polar grid projection (Madec & Imbard, 1996) and covers the North West Atlantic at a nominal 1/36° horizontal resolution (NWA36), corresponding to an average grid spacing of about 2 km. The model covers the area from Cape Hatteras at its southern boundary (~35°N) to the southern part of Labrador (~54°N) and

https://doi.org/10.5194/egusphere-2023-42
Preprint. Discussion started: 26 January 2023
© Author(s) 2023. CC BY 4.0 License.

from the coast to 35°W. This allows the model to incorporate key areas such as the Gulf Stream separation region, the Grand Banks of Newfoundland, the Gulf of St. Lawrence, the Scotian Shelf and the Bay of Fundy.

The reference bathymetric dataset for the deep ocean is interpolated from the global dataset of Smith and Sandwell (SRTM30_plus version 11; Becker et al. 2009). Over the Scotian Shelf, the Gulf of Maine and the Bay of Fundy, the bathymetry field is re-interpolated from the high-resolution data used in the Gulf of Maine – Scotian Shelf model (GoMSS; Katavouta et al. 2016). Over the GSL, the background bathymetry information is supplemented with additional sounding information collected by DFO. Due to the presence of the world's largest tidal range, reaching 16 m in the upper Bay of Fundy, and because NEMO v3.6 does not include a wetting-drying scheme, a minimum depth of 7.5 m is imposed over the model domain to ensure no ocean point would dry out. The area around and in Minas Basin at the upmost region of the Bay of Fundy had to be deepened to a minimum of 7.5 m while changes to the basin's geometry were made to approximately conserve its total volume. This limitation will be removed in future CIOPS-E versions that will use an updated NEMO version (4 or more recent) that includes a wetting-drying scheme to deal with inter-tidal zones.

3.1.3 Ocean Open Boundary Conditions

The model is forced at its open boundaries with daily-averaged three-dimensional fields for temperature, salinity, and non-tidal velocities and sea surface height (SSH) from RIOPS (Smith et al. 2021), and tidal velocities and SSH calculated from tidal harmonic constants. At the locations of the CIOPS-E open boundaries, the hourly SSH from RIOPS is de-tided using the ECCC online harmonic analysis tool (described in Smith et al. 2021) before daily averages are computed. Linear interpolation is used between daily averaged values to avoid creating shocks. Tidal forcing is imposed at the lateral boundaries using elevation and barotropic transports of 13 constituents (M2, S2, N2, K2, K1, O1, P1, Q1, Mf, Mm, M4, MS4 and MN4), with the data taken from the Oregon State University TPXO tidal model (Egbert and Erofeeva, 2002). The prescribed self-attraction and loading terms are interpolated from the Finite Element Solution (FES 2012) tidal product (Carrère et al. 2012). The radiation scheme of Flather (1976) is applied to obtain the barotropic current normal to the lateral open boundaries, using SSH and barotropic transports from the sum of non-tidal and tidal components.

3.1.4 River runoffs and the St Lawrence 1D model

Except for the St. Lawrence River, the river runoff contributing to CIOPS-E are derived from climatological data. The monthly climatologies of runoff are based on observations from the 28 most important tributaries in the GSL (Saucier et al., 2003), and the data of Dai and Trenberth (2002) outside of the GSL. The monthly climatologies are further interpreted to daily values and applied to the ocean model as a surface volume flux (similar to precipitation) at the ocean model point closest to the river outlet. The freshwater discharge is assumed to be at the same temperature as the surface ocean temperature.

The St. Lawrence river is the largest source of freshwater over the model domain, with an annual mean discharge of 11 x 10^3 m^3 s^{-1} (Bourgeault and Koutitonsky, 1999) and a spring freshet that often exceeds 20 x 10^3 m^3 s^{-1}. The ocean model domain reaches the vicinity of Québec City (Fig.1) where the water level is still influenced by tides. To alleviate complexities of both

https://doi.org/10.5194/egusphere-2023-42
Preprint. Discussion started: 26 January 2023
© Author(s) 2023. CC BY 4.0 License.

the freshwater flux and to absorb the energy of the incoming tides, CIOPS-E uses a one-dimensional model for the St. Lawrence river (Dronkers, 1969). The daily freshwater discharge (in $m^3 s^{-1}$) is obtained from the DFO real-time estimate (Lefaivre et al., 2016). In the event that the daily freshwater discharge is not available, the model calculates the daily runoff from a pre-defined runoff climatology.

3.1.5 Mesoscale correction method (Spectral nudging)

Besides providing the forcing at the lateral open boundaries, the RIOPS data assimilative solution is also used to constrain the CIOPS-E large-scale three-dimensional temperature and salinity fields. This is achieved using the spectral nudging method (Thompson et al., 2006) that is applied for wavenumbers of meso-scale eddies and lower. These scales are well constrained in the RIOPS solution by using the sophisticated data assimilation scheme. In higher wavenumber bands, CIOPS-E solution is free to evolve and to generate unconstrained finer-scale features. Spatially, the spectral nudging is applied only offshore of the 1500 m isobath, where sufficient observational data is available to constrain the RIOPS solution. Over the shelf and coastal areas, CIOPS-E is unconstrained to allow the solution to benefit from the improved representation of the coastline, bathymetry and higher resolution atmospheric forcing.

To evaluate the effectiveness of the spectral nudging method in constraining CIOPS-E mesoscale features, we evaluate the SSH anomaly between satellite-retrieved observational datasets, RIOPS, the standard CIOPS-E experiment and complemented with an additional *free-run* CIOPS-E experiment. In the latter, the spectral nudging is deactivated, allowing the model solution to evolve freely without constraints towards ocean observations. Figure 2 compares the SSH anomalies along a specific altimeter track (#226 from Jason 2) and the different RIOPS and CIOPS-E solutions. Satellite altimetry observations are obtained from the AVISO Salto/Duacs near-real time along-track product. The track 226 extends from the Avalon Peninsula in Newfoundland, over the Grand Banks before crossing the eddy energetic region of the Gulf Stream. The satellite altimetry and RIOPS are well correlated in time and shows similar amplitudes of the SSH anomalies. The close correspondence shows the efficiency of RIOPS data assimilation in constraining the location and amplitudes of the large-scale eddies (Smith and Fortin, 2021). The standard CIOPS-E simulation using the spectral nudging offshore also reproduces to a large extent the observed mesoscale variability. The CIOPS-E *free-run*, on the other hand, is not constrained to reproduce the individual eddies and therefore represents an expression of the inherent chaotic nature of the ocean system.

Additionally, the comparison of model solutions with gridded altimetry sea surface anomaly data (Fig. 3) demonstrates clearly the efficiency of the data assimilation method in RIOPS to reproduce the Gulf Stream eddies' strength and location. Figure 3 also confirms the efficiency of the spectral nudging to correct the large-scales in CIOPS-E for the entire offshore portion of the model domain.

3.2 Sea Ice model

In CIOPS-E, NEMO is coupled to the Los Alamos Community Ice CodE version 4 (CICE4; Hunke 2001; Lipscomb et al., 2007; Hunke and Lipscomb, 2008). CICE represents the sea ice dynamics using an elastic-viscous plastic scheme and

https://doi.org/10.5194/egusphere-2023-42
Preprint. Discussion started: 26 January 2023
© Author(s) 2023. CC BY 4.0 License.

thermodynamics over ten ice thickness categories, three ice vertical layers and a single snow layer. CICE uses the seabed stress approach to parameterize landfast ice following Lemieux et al. (2015, 2016b). The principal ice parameters are consistent with RIOPS (Dupont et al. 2015). The ice-ocean drag coefficient is computed by a log-layer assumption following Roy et al. (2015). The ice strength parameters P* and C* are 27.5 kN/m^2 and 20 respectively. No sea ice open boundary conditions are provided at the northern boundary and therefore the sea ice advected from the Labrador Shelf is neglected. A future version of the CIOPS-E system will include the Labrador Shelf ice flux.

3.3 Atmospheric forcing

The ocean model is forced at the surface by hourly fields from the Canadian Numerical Weather Prediction Model Global Environmental Multiscale (GEM; Côté al. 1998). Forcing variables include hourly winds, air temperature and specific humidity at the lowest prognostic level of the atmospheric model (~40 m), precipitation and surface downward short- and long-wave radiation. Forcing due to atmospheric pressure is also included in the ocean momentum equation to include the inverse barometer effect on the ocean's surface. Two configurations of the GEM model are combined to cover the entire CIOPS-E domain. The majority of the ocean domain is covered by the High Resolution Deterministic Prediction System (HRDPS; Milbrandt et al. 2016) with a grid resolution of 2.5 km. As the southeastern part of the ocean domain is not covered by the HRDPS, the HRDPS fields are combined with those from the Global Deterministic Prediction System (GDPS; Gasset et al. 2019; 15 km grid resolution). To avoid creating unphysical changes in the atmospheric fields at the junction of the two grids, a spatio-temporal blending technique is used. In brief, from the southeastern limit of the ocean grid inward, a weighted average over a transition area of 100 grid points (~250 km) is performed where the GDPS solution is gradually replaced by that from the HRDPS. To create a continuous time series of forcing fields for CIOPS-E pseudo-analysis component (described in next section), a simple temporal blending method is used. The temporal method is a simple linear combination between the forecast hours 06-17 from the previous 00Z and 12Z runs in both GDPS and HRDPS, similar to the method used by Bernier and Thompson (2015). As the CIOPS-E forecast is forced with the 48h forecasts from HRDPS/GDPS, no time interpolation is required (see next section).

3.4 CIOPS-E system components

CIOPS-E has two components, a pseudo-analysis and a forecast component (Fig. 4). The pseudo-analysis (PA) runs each day for 24h. The previous PA daily run provides the initial conditions for the ocean and sea ice fields. Ocean lateral boundary conditions are provided from the daily-averaged RIOPS forecast component (RIOPS-F). The spectral nudging method described in Section 3.1.5 is used to constrain the large-scale temperature and salinity fields offshore of the 1500 m isobath. The sea ice fields are unconstrained in the PA, allowing the ice and ocean fields to interact while avoiding any accumulation of errors associated with imbalances caused by the assimilation of sea ice information.

The forecast component (CIOPS-E F) produces 48h forecasts four times per day at 00Z, 06Z, 12Z & 18Z. The ocean initial conditions are provided by the PA component for the 00Z forecast and by a restart file written at hour 06 of the previous

https://doi.org/10.5194/egusphere-2023-42
Preprint. Discussion started: 26 January 2023
© Author(s) 2023. CC BY 4.0 License.

forecast for the 06Z, 12Z and 18Z executions. The daily-averaged RIOPS boundary conditions in the forecasts are taken from the previous available forecast, with a persistence of the variables over the hours 25-48 of CIOPS-E forecast. The sea ice conditions in the forecast component are initialized via a direct insertion of total ice concentration analyses from the Regional Ice Prediction System (RIPS; Buehner et al., 2013, 2016). RIPS uses a 3DVar approach on a 5-km resolution grid assimilating satellite observations and CIS charts and Radarsat2 image analyses. The Rescaled Forecast Tendencies (RFT) method of Smith et al. (2016) is used to adjust the ten ice thickness categories based on the total ice concentration analysis. Note that the same approach is used by RIOPS, but differs from that used in RMPS-GSL. In the RMPS-GSL, ice concentration is constrained using direct insertion of Radarsat2 image analyses, with an additional constraint on ice thickness based on "Stage of development" (Smith et al., 2013).

4. Model evaluation

The CIOPS-E evaluation is performed using a 1-year pseudo-analysis run between March 1st 2019 and February 29th 2020. The simulation is initialized in November 2015 and runs continuously up to the evaluation period. As the operational atmospheric model changed significantly in 2018, impacting the near-surface and radiation fields, we focus our analysis of the CIOPS-E results after the atmospheric model's update. Model evaluation focuses on variables important for simulation of oil drift and fate and behaviour, namely (i) the representation of the tidal amplitude and phase, (ii) subtidal water level variability, (iii) sea surface temperature, (iv) water mass properties and (v) seasonal sea ice cover.

Inter-model comparisons are presented with several other CCMEP operational products and systems, as noted above. These include the CCMEP SST analysis and two forecasting systems, namely RIOPS and RMPS-GSL.

4.1 Tides

Evaluation of the tidal amplitudes and phases presented in this section is based on results from a harmonic analysis performed using the t-tide package (Pawlowicz et al., 2002) on hourly time series observed water levels at selected tide gauges as well as on simulated sea surface height. The harmonic analysis is performed on the closest model wet point to the tide gauge location. The harmonic analysis is performed over the period from March 1st 2019 to February 29th 2020. Additional comparisons between the observed and CIOPS-E tidal amplitudes and phases for the main five tidal constituents (M2, N2, S2, K1 and O1) at all stations are presented in Paquin et al. (2021, 2022).

Figure 5 presents the co-amplitude and co-phase for the principal lunar semidiurnal tidal constituent (M2) comparisons for OSU, CIOPS-E, RIOPS and RMPS-GSL. OSU is used here as a reference for comparison as it also provides the tidal boundary conditions for CIOPS-E. The main M2 features over the region are (i) the M2 resonance in the Bay of Fundy (saturated colours) leading to tidal range up to 16 m in the upper bay, (ii) the large amplitudes along coast of the Gulf of Maine, (iii) the amphidrome located in the central GSL close to the Îles-de-la-Madeleine (station #10 on Fig.1) and (iv) the increasing amplitude along the St. Lawrence Estuary. Figure 5 shows a general improvement of the M2 tides in both amplitude and phase

https://doi.org/10.5194/egusphere-2023-42
Preprint. Discussion started: 26 January 2023
© Author(s) 2023. CC BY 4.0 License.

in CIOPS-E compared to RIOPS. CIOPS-E reproduces the larger tidal amplitudes and also corrects the phase errors in the Bay of Fundy and Gulf of Maine area seen in RIOPS. The location of the amphidrome in the Central GSL is clearly improved in CIOPS-E compared to RIOPS. Tidal amplitudes and phases across the GSL are also better represented. The Northeastern Gulf shows better agreement in amplitudes between CIOPS-E and OSU, while RIOPS overestimates tidal amplitudes. The increasing amplitudes along the St. Lawrence Estuary is also better represented in CIOPS-E as RIOPS tends to overestimate the signal. Although the tidal amplitudes are similar between CIOPS-E and the RMPS-GSL, CIOPS-E significantly improves the M2 phases. Similar results are obtained for the other semi-diurnal constituents (Paquin et al. 2021, 2022). CIOPS-E reproduces the resonant system for the semi-diurnal tides in the Gulf of Maine and Bay of Fundy despite an overestimation of the M2 amplitudes. The overestimation of M2 reaches a maximum of 30 cm at the St. John Harbour (#19) and Eastport (#20) coastal tide gauges, where it represents about 10% of the M2 amplitude (see Fig. 7 presented later).

Similar comparison of the tidal amplitude and phase for the lunar diurnal constituent (K1) is presented on Figure 6. Generally, CIOPS-E simulates larger K1 amplitudes in the GSL, improving with respect to the underestimated RIOPS amplitudes. CIOPS also reproduces the observed increase in K1 amplitude in the Northumberland Strait, absent in RIOPS and OSU. Phases, however, are slightly degraded in the GSL by up to 5° (~20 minutes) compared to RIOPS.

In general, the improvements of the tides compared to RIOPS and RMPS-GSL are due to multiple factors: (i) the application of tidal boundary conditions closer to the region of interest compared to RIOPS[1] but (ii) also due to a refined resolution of the coastline and addition of higher resolution and more accurate bathymetric data, especially for the GSL and the St. Lawrence Estuary.

At coastal tide gauges, quantitative differences between modelled and observed tides are calculated using the complex differences (Foreman et al. 1995), defined as:

$$D = [(A_O \cos g_O - A_M \cos g_M)^2 + (A_O \sin g_O - A_M \sin g_M)^2]^{1/2} \quad (2)$$

where A_O, A_M, g_O and g_m are the observed and modelled amplitudes and phases, respectively. Figure 7 compares the complex differences calculated at the coastal tide gauges for M2 and K1 tidal constituents for CIOPS-E, RIOPS, RMPS-GSL and OSU. Stations are organized from the Upper St. Lawrence Estuary, through the GSL, around Newfoundland, the Bay of Fundy – Gulf of Maine, ending southward along the East Coast of the United States.

CIOPS-E improves the representation of the M2 tides with smaller complex differences compared to RIOPS and RMPS-GSL for all but one station. The improvements of the M2 complex difference between CIOPS-E over RIOPS is especially important over the GSL and the Estuary, where improved representation of the bathymetry and coastline, combined with the adjusted bottom friction significantly improves the propagation of the tides and the location of the amphidrome. Despite a significant improvement of the complex differences in the Bay of Fundy – Gulf of Maine area compared to RIOPS (stations 18 to 22), large errors are still noted in the CIOPS-E complex differences, due mostly to an overestimation of the M2 amplitudes (also visible on Fig.5). We suspect these errors are due to the lack of details in the representation of the complex coastline and

[1] RIOPS's domain covers from 26°N in the North Atlantic to 44°N in the North Pacific (Smith et al. 2021).

https://doi.org/10.5194/egusphere-2023-42
Preprint. Discussion started: 26 January 2023
© Author(s) 2023. CC BY 4.0 License.

bathymetry of the tidal resonant system, amplified by the modifications applied to the minimum model water depth necessary by the absence of a wetting-drying scheme in the current NEMO version. We expect significant improvements resulting from the addition of the scheme in the future versions of the CIOPS-E system.

For K1, reduction of the complex differences in CIOPS-E are also noted compared to RIOPS and RMPS-GSL for most stations. Besides the improvements in the upper St. Lawrence, CIOPS-E also better represents the K1 tide in the Northumberland Strait (between Prince Edward Island and the mainland), namely the Shediac Bay (#8) and Charlottetown (#9) tide gauges, due to improved resolution of the coastline and updated bathymetry in the 1/36° grid. One might note the improved skills over the OSU model for both stations, where CIOPS-E clearly has smaller errors. Improvement in the K1 phase in CIOPS-E explains the general improvement of the complex difference scores compared to the RMPS-GSL.

4.2 Sub-tidal water levels

In this section, we compare the modelled residual water levels and its variability from CIOPS-E, RIOPS and RMPS-GSL with observations at the selected coastal tide gauges (Fig. 1). The residual water levels are calculated by removing the tidal reconstruction using the harmonic analysis coefficients from t-tide. The mean water level at each station is removed for observations and models. As previously presented, the harmonic analysis is performed over the standard 1-year period from March 1st 2019 to February 29th 2020.

Figure 8 shows the daily averaged residual water levels at three selected coastal tide gauges: Rimouski (#3) in the St Lawrence Estuary, Saint John Harbour (#19) in the Bay of Fundy and St. John's (#14) in Newfoundland. Both RIOPS and CIOPS-E reproduced the seasonal variability with larger variability in winter compared to summer, associated with the stronger winter storms and atmospheric synoptic systems. Summertime variability is reduced in both the models and the observations. Comparison of the power spectrum (not shown) confirms that more energy is present in the observations and RIOPS over the 10-day atmospheric synoptic frequency band as compared to CIOPS-E. This lack of energy around the 10-day frequency band is deemed outside the scope of this paper but will be the focus of future investigation.

The RMPS-GSL model does not capture the timing nor the amplitude of the residual water level at the Rimouski tide gauge (#3) and other stations within the model domain (not shown). The RMPS-GSL model uses climatological boundary conditions at the Belle-Isle and Cabot Straits, therefore lacking the storm surge signal generated in the North Atlantic that should propagate into the GSL. Moreover, the inverse barometer effect on the model's sea surface is not included in the RMPS-GSL, resulting in the large underestimation of the locally-generated residual water level variability. As the RMPS-GSL system was developed to better represent the atmosphere-ocean-sea ice interactions over the GSL in an atmospheric forecasting context, the representation of the residual water levels was not the focus during its development. Nevertheless, as the CIOPS-E is used as the updated ocean configuration in the new Water Cycle Prediction System (WCPS; Durnford et al. 2018) and given that the CIOPS-E pseudo-analysis provides initial conditions for the WCPS, an evaluation against the former RMPS-GSL model and demonstration of the improved quality of the residual water levels is necessary prior to the change in operational products.

https://doi.org/10.5194/egusphere-2023-42
Preprint. Discussion started: 26 January 2023
© Author(s) 2023. CC BY 4.0 License.

Figure 9 presents a domain-wide quantitative evaluation of the daily averaged residual water levels for the different modeling systems using the root-mean-square errors and the gamma-square score (γ^2). The gamma-square score (Thompson et al. 2003, Bernier and Thompson 2010) is defined as the variance of the difference between observation and modelled prediction divided by the variance of the observations. A perfect model would have a score of zero and a score of 1 indicates that the modeling system is no better than using a constant value (or persistence).

Generally, both CIOPS-E and RIOPS present smaller root-mean square errors and gamma-square scores for the daily-averaged residual water levels over the East Coast of the United States. Errors in the daily residual water levels then increase for the Bay of Fundy and reach maximum values in the GSL and Estuary. Table 2 presents the RMSE, correlation and gamma-square scores for each coastal tide gauge.

CIOPS-E shows smaller errors compared to both RIOPS and RMPS-GSL. The improvements are clearly visible for the Bay of Fundy, where RIOPS is limited in its representation of the Bay's geometry due to its coarser resolution. Similar conclusions are shown for the Northumberland Strait, with improvements to the Charlottetown and Shediac Bay stations. Significant improvements are also visible in the GSL, where CIOPS-E shows significant improvements compared to both RIOPS and the RMPS-GSL. As previously mentioned, the RMPS-GSL shows the largest errors for all stations across the GSL as it poorly represents the synoptic variability of the residual water levels. Despite significant improvements in CIOPS-E, both CIOPS-E and RIOPS show similar error structure with larger errors in Cap-aux-Meules, Îles-de-la-Madeleine (#10), increasing at the eastern Gaspé Peninsula station in Rivière-au-Renard (#5) and also at Rimouski (#3). This error is likely linked with errors in the steric structure related to the representation of the Gaspé Current. Both CIOPS-E and RIOPS also show their largest errors at their uppermost station in the St. Lawrence Estuary, namely the St-Joseph-de-la-Rive (#2) for RIOPS and Saint-François-de-l'Île-d'Orléans (#1) for CIOPS-E, linked with the interactions between the upstream propagation of the storm surge signal with the 1-D river model used to represent the St. Lawrence River. The impact of the limited resolution also plays a role in decreasing the precision of the model to represent the complex interactions further up in the estuary such as the interaction with the St. Lawrence freshwater plume, the complex bathymetry and the mixing occurring at the head of the Laurentian Channel. The modelled winds might also present a source of error in this area as the St. Lawrence valley widens and will be evaluated in more details in an upcoming study.

4.3 Sea surface temperature

We next evaluate the model capability to reproduce the seasonal averaged SST. Figure 10 presents the average SST for two periods, (i) spring (April to June) and (ii) fall (October to December). Modelled SST are compared to the CCMEP SST analysis. Note that the CCMEP SST analyses are assimilated in RIOPS and applied as surface boundary conditions for atmospheric prediction systems used here.

Offshore, the SST differences are very similar between RIOPS and CIOPS-E, clearly demonstrating the efficiency of the spectral nudging method applied in CIOPS-E to constrain the SST towards RIOPS's solution. Differences are larger near the

https://doi.org/10.5194/egusphere-2023-42
Preprint. Discussion started: 26 January 2023
© Author(s) 2023. CC BY 4.0 License.

shelf break, where the spectral nudging is relaxed to reach zero on the shelf. The shelf break region is also energetic and chaotic in nature, allowing for some expression of the unconstrained internal model variability.

On the shelf, differences are generally larger in CIOPS-E compared to RIOPS. The larger differences are expected as RIOPS assimilates the CCMEP SST analysis in the data assimilation procedure, including over the shelf region. Despite the direct assimilation of satellite and in situ observations in the CCMEP SST analysis, some small-scales features are more clearly defined in the models compared to the CCMEP SST. Such features include the representation of both the inshore and offshore branches of the Labrador Current, visible as colder differences in both RIOPS and CIOPS-E. CIOPS-E also simulates a stronger and colder current along the northern section of Orphan Basin, a feature absent from the CCMEP SST and weaker in RIOPS.

Over the GSL, models generally tend to be colder (warmer) than the CCMEP SST analysis during spring (fall). As expected due to the use of data assimilation, differences are smaller in RIOPS and slightly larger in CIOPS-E, especially over the Magdalen Shallows. All models also feature warmer waters around the Îles-de-la-Madeleine in spring, a local maximum related to the shallow waters around the archipelago, completely absent in the CCMEP SST analysis. Compared to an early version of the CIOPS-E system (Paquin et al. 2022), the adjustment of the vertical mixing significantly improves the biases over the GSL area, especially in summer, reducing from a 4°C bias to less than 2°C.

Over the Scotian Shelf, Bay of Fundy and Gulf of Maine, CIOPS-E is generally warmer compared to RIOPS. The exact causes of the warm differences are still under investigation but two current working hypotheses points towards 1) an underrepresentation of the low level clouds and fog in the atmospheric forcing, leading to an overestimation of the shortwave radiation at the surface, warming the near-surface waters during the summer; 2) CIOPS-E does not adequately represent the upwelling region located at the southwest of the Nova Scotia and the tidally rectified circulation around Georges Bank. Future studies will focus on the water mass properties and intensity of the Scotian Current and pathways in and around the Bay of Fundy – Gulf of Maine areas.

4.4 In situ temperature and salinity

The water masses in the St. Lawrence Estuary are influenced by the discharge from the St. Lawrence River plume forming a surface-intensified buoyant coastal current flowing along the south shore of the estuary. The current, referred as the Gaspé Current, can become baroclinically unstable (Reszka and Swaters, 1999) and detach from the coast to partially recirculate cyclonically in the Anticosti Gyre (Sheng 2001; Saucier et al. 2003). In the estuary, tides generate mixing between the warm and salty Bottom Atlantic Layer (BAL) and the Cold Intermediate Layer (CIL) at the head of the Laurentian Channel, also influencing the water properties. The CIL, located generally between 50-150 m is partially generated locally in the Gulf during the winter but also advected from the Labrador Shelf through Belle-Isle Strait and circulating in the Gulf (Koutitonsky & Budgen, Saucier et al. 2003, Smith et al. 2006a, Smith et al 2006b). All these processes affect the water properties recorded at the IML-4 buoy location, near Rimouski (see fig.1). The IML-4 buoy is part of the DFO ocean monitoring programs, which

https://doi.org/10.5194/egusphere-2023-42
Preprint. Discussion started: 26 January 2023
© Author(s) 2023. CC BY 4.0 License.

maintains several important long-term buoys in the St. Lawrence Estuary and GSL areas. Of the available buoys, the IML-4 buoy has the longest records of temperature and salinity profiles, with minimal data gaps between April and November 2019. Figures 11 and 12 show the evolution from April to November 2019 of the temperature and salinity profiles, respectively. The winter profiles show a surface mixed layer and CIL extending from the surface to about 100 m lying above the warmer and saltier BAL. The observed profiles show the transition in spring from the two-layer system to a three-layer system with the spring warming and freshening of the near-surface layer.

The difference plots shows that both the CIOPS-E and RMPS-GSL models tend to reproduce the general structure and evolution of the water masses at IML-4. Both models also show a warm and salty bias around 25 m, most likely resulting from a lack of vertical mixing due to the over-stratification of the surface layer. However, the near-surface cold and fresh biases are improved in CIOPS-E in comparison with the RMPS-GSL model.

Below the surface layer, CIOPS-E better represents the formation and persistence of the CIL with smaller biases from June to November, although some erosion of the CIL, visible as a developing warm bias at depth, does occur over time. The current hypothesis for the erosion is a stronger tidal mixing at the head of the Laurentian Channel in CIOPS-E, strengthening the estuarine circulation and eroding the CIL with BAL. The presence of the salty bias in CIOPS-E below 150 m and the mixed condition in the upper estuary (not shown) tend to support this hypothesis. A sensitivity experiment of CIOPS-E water masses in the estuary to mixing is currently in progress to provide more detailed explanation and will be the topic of a subsequent study. The mid-May 100 m warm bias present in both models might be caused by the misrepresentation of an advective event of CIL waters visible in the observed temperature profiles. One might also note that the comparison of the model temperature and salinity to a timeseries at a single point location is subject to spatial aliasing and highlights the challenges of performing a thorough evaluation in a data-sparse environment.

4.5 Sea ice

The sea ice evaluation is performed against the RMPS-GSL system, used to provide operational sea ice cover and thickness forecasts to end-users, such as the Canadian Ice Service (CIS). The sea ice in CIOPS-E's pseudo-analysis is not constrained and evolves freely over the ice season. In the CIOPS-E forecasts, the sea ice cover is adjusted using the RIPS ice concentration analyses (as described in Section 3.2). Figure 13 compares the evolution of the sea ice concentration and thickness over the 2020 winter season along with the average biases against the CIS Radarsat image analyses. The evolution of the sea ice cover shows an overestimation of the concentration in the CIOPS-E pseudo-analysis. The overestimation of sea ice concentration is significantly reduced in the forecast component due to the insertion of the RIPS analyses, thereby providing similar scores to the RMPS-GSL. As the RMPS-GSL assimilates the same Radarsat image analyses as used for the evaluation, this comparison is obviously not independent but is intended to show the quality and limitation of the system in its current configuration. This is especially true as the CIOPS-E ocean configuration is now used in the WCPS, replacing the RMPS-GSL system as the operational system.

https://doi.org/10.5194/egusphere-2023-42
Preprint. Discussion started: 26 January 2023
© Author(s) 2023. CC BY 4.0 License.

For sea ice thickness, both the CIOPS-E pseudo-analyses and forecasts show significantly larger biases over the 2020 winter when compared to the RMPS-GSL. The RMS increases in both the pseudo-analysis and the forecast components of the system over the winter and at a faster rate compared to the RMPS-GSL. The ice thickness comparison uses Radarsat "stage of development" as a proxy for thickness and is not a direct comparison. Moreover, as the RMPS-GSL system uses this same data source for initialization of its sea ice variables, smaller biases are to be expected. The CIOPS-E forecast shows an overestimation of the average sea ice thickness as no correction are applied to the thickness (only sea ice concentration).

Figure 14 presents the sea ice thickness bias over the Gulf area between CIOPS-E and the RMPS-GSL, both compared to the Radarsat estimates. As expected, the ice thickness differences are generally larger in CIOPS-E compared to the RMPS-GSL, as RMPS-GSL uses the Radarsat thickness estimates to constrain the model. In the absence of an independent source of observational data, the comparison still allows an evaluation of the CIOPS-E differences and to a lesser extent of the absolute accuracy of the new system. As an example, the pattern of thickness overestimation in CIOPS-E shows thicker ice along the southern coast of the St. Lawrence Estuary, mostly in the Bas-St-Laurent and Gaspésie regions. As the Radarsat thickness estimates are performed manually using a polygon-based approach, small-scale features such as the dynamical accumulation of thicker and more deformed ice along the coast is not properly represented in the observational estimates. Additionally, the thickness estimates from CIS relies on a thermodynamic growth estimate not taking into account the ice convergence. As such, a quantitative estimate of the sea ice thickness errors is not feasible using this dataset. A similar situation might be happening in the Northumberland Strait and in the Strait of Belle-Isle.

5. Summary and Conclusions

The Coastal Ice-Ocean Prediction System for the East Coast of Canada (CIOPS-E) was developed and implemented at CCMEP to respond to the growing demand for modeling support for aquatic emergency response, hazards in ice-infested waters and in support of other CONCEPTS applications (e.g., Search and Rescue and National Defense). CIOPS-E is also a complementary coastal model playing a central role in the Ocean Protection Plan to provide model results in support of electronic navigation and open boundary conditions for the different sub-kilometer port-scale ocean models currently in development for the Canadian East Coast by Fisheries and Oceans Canada.

The CIOPS-E domain covers most of the East Coast of Canada, from the Gulf of Maine to the southern Labrador Shelf and includes the Gulf of St. Lawrence. The spectral nudging method applied offshore of the shelf break is shown to effectively constrain the large-scale temperature and salinity fields towards the data assimilative solution from RIOPS. This allows the reproduction of the observed eddy structure and overall large-scale circulation, otherwise impossible considering the model's internal variability.

Tidal and sub-tidal water levels in CIOPS-E are significantly improved compared to RIOPS and RMPS-GSL. The improvements are especially important for the semi-diurnal tides in the Bay of Fundy and in the Gulf of St. Lawrence. In the Gulf, CIOPS-E improves the location of the amphidrome at the Îles-de-la-Madeleine, therefore improving both amplitudes

https://doi.org/10.5194/egusphere-2023-42
Preprint. Discussion started: 26 January 2023
© Author(s) 2023. CC BY 4.0 License.

and phases across the whole region. In the Gulf of Maine – Bay of Fundy area, the resonant system of the semi-diurnal tides are also greatly improved in CIOPS-E compared to RIOPS, despite showing larger errors compared to the Gulf of St. Lawrence. A future version of the NEMO system including a wetting and drying scheme should eventually allow improvements of tides in this challenging region.

Both RIOPS and CIOPS-E reproduce the seasonal variability of the sub-tidal water levels with larger variations associated with the more intense wintertime atmospheric synoptic systems. CIOPS-E shows overall improvement in the representation of residual (sub-tidal) water levels for most stations compared to RIOPS. The improvement is especially important for areas where the increased horizontal resolution in CIOPS-E allows for a more accurate representation of the complex coastline combined with more accurate bathymetry data, such as in the Bay of Fundy and Northumberland Strait.

A comparison with the CCMEP SST analysis shows a persistent summertime cold bias over most of the "free zone" in CIOPS-E (i.e. where no spectral nudging is applied). Combined with the analysis of in situ temperature and salinity profiles, the cold surface bias appears to be a consequence of insufficient vertical mixing near the surface in CIOPS-E. Despite these limitations, CIOPS-E does improve the overall representation of the water masses and the persistence of the CIL for the IML-4 buoy located in the St. Lawrence Estuary when compared to the RMPS-GSL system.

The evaluation of the sea ice cover and thickness presented in this study allows for a qualitative evaluation of the differences between the RMPS-GSL and CIOPS systems. As the RMPS-GSL is constrained by the same Radarsat image analyses, the differences presented here are not intended to provide an absolute measure of the thickness biases in the Gulf. Nevertheless, the spatial comparisons of sea ice cover and thickness with the Radarsat-based estimate shows that CIOPS-E produces thicker ice in areas of known sea ice deformation, such as the wind compaction of deformed ice along the south shore of the St. Lawrence estuary. The sea ice analysis also emphasizes the challenges of producing a detailed bias estimation in the absence of independent high-resolution datasets. Future work should address these challenges with more in-depth studies of the ice season (onset, duration and melt) over the Gulf of St. Lawrence using longer simulations and diverse sea ice datasets.

In conclusion, the evaluation of CIOPS-E with respect to the near-surface variables directly affecting the currents and water level represents significant improvements over RIOPS and RMPS-GSL, therefore providing a source of high-quality reliable estimates of ocean conditions in the northwest Atlantic Ocean capable of supporting a variety of high-impact operational applications.

This study also clearly demonstrates the areas of improvement where we should invest energy to correct some of the system's limitation. For instance, the addition of the wetting-drying capacity in future NEMO development should eventually be incorporated in the CIOPS-E future version, allowing a reduction of the errors noted in areas such as the Bay of Fundy. Work is also is currently in progress to evaluate the interannual variability of CIOPS-E over a longer period by performing hindcast simulations, covering 1992-present. These experiments will allow us to expand our possibilities of data-model comparison by

https://doi.org/10.5194/egusphere-2023-42
Preprint. Discussion started: 26 January 2023
© Author(s) 2023. CC BY 4.0 License.

using observational data collected by different long-term monitoring programs such as DFO's Atlantic Zone Monitoring Program[2]. Furthermore, the hindcast also allows the evaluation of modelled trends compared to the observed trends.

Investigation of CIOPS-E circulation anomalies and CIL formation sensitivity to different resolution of atmospheric forcing is also currently underway. Using the WCPS framework will also allow us to evaluate the potential benefits of using a fully coupled ocean-sea ice-atmosphere system on the quality of forecasts. Emphasis on extreme events (cold air outbreaks, strong synoptic low pressure systems and hurricanes) over the ice-covered Great Lakes and Gulf of St. Lawrence, should allow us to detect the impact of more realistic evolution of surface conditions in the fully-coupled ocean-sea ice – atmosphere model and the potential to improve the meteorological forecasting capacity.

Finally, ongoing model development is also required to gradually fill-in the gaps in the current ocean-sea ice forecasting system with the objective to develop a more comprehensive model of the coastal environment, in agreement with international research groups and programs such as COSS-TT (Cirano et al. 2021), Coast Predict[3] and the general consensus on coastal model development (Fringer et al. 2021). Such improvements of varying level of complexity range from using more realistic ocean colour data, to coupling with a land-hydrology model for river discharge (and eventually river water temperature), to the addition of wave-ocean processes in the model via a forced or coupled approach. Coastal data assimilation should also eventually be added to the forecasting model in order to better constrain CIOPS-E solution over the shelf.

6. Author contributions

FR, GCS, SM, FD, YL and JPP developed the system configuration. SSOD contributed to high resolution model bathymetry. FR, SM, JL, FD and JPP contributed to the operational implementation of the system. All authors contributed to the system evaluation. JPP prepared the manuscript. FR, GCS, FD, YL, ST, SSOD, NS and MD reviewed the manuscript.

7. Competing interests

The authors declare that they have no conflict of interest.

8. Acknowledgments

The authors acknowledge the support from the Canadian inter-departmental CONCEPTS program. We would like to thank all the employees of the Research, Prediction Development and Operations divisions of the Canadian Centre for Meteorological

[2] AZMP website: https://www.dfo-mpo.gc.ca/science/data-donnees/azmp-pmza/index-eng.html
[3] https://www.coastpredict.org/

https://doi.org/10.5194/egusphere-2023-42
Preprint. Discussion started: 26 January 2023
© Author(s) 2023. CC BY 4.0 License.

and Environmental Prediction who contributed to this project in all of its various aspects: systems development and evaluation, maestro suites, technological transfer to operations, run evaluations and management of the project evolution.

We would also like to thank Department of Fisheries and Oceans colleagues, including Xianmin Hu, Doug Schillinger, and Yvonnick Le Clainche for help with model development and evaluation, and others involved in different monitoring programs to collect the *in-situ* observational data used for model evaluation. Finally, we would like to thank help and advices from Mercator-Ocean International, and in particular, Jérôme Chanut.

9. References

Aguiar, E., Mourre, B., Juza, M. *et al. :* Multi-platform model assessment in the Western Mediterranean Sea: impact of downscaling on the surface circulation and mesoscale activity. Ocean Dynamics, 70, 273–288. https://doi.org/10.1007/s10236-019-01317-8. 2020

Becker, J. J., Sandwell, D.T., Smith, W. H. F., Braud, J., Binder, B., Depner, J., Fabre, D., Factor, J., Ingalls, S., Kim, S-H., Ladner, R., Marks, K., Nelson, S., Pharaoh, A., Trimmer, R., Von Rosenberg, J., Wallace, G. and Weatherall, P. : Global Bathymetry and Elevation Data at 30 Arc Seconds Resolution: SRTM30_PLUS, Marine Geodesy, 32:4, 355-371, 2009.

Bélair, S., Méthot, A., Mailhot, J., Bilodeau, B., Patoine, A., Pellerin, G. and Coté, J.: Operational implementation of the Fritsch–Chappell convective scheme in the 24-km Canadian regional model. Wea. Forecasting, 15**,** 257–274, 2000.

Bernier, N.B., and Thompson, K.R. : Tide and Surge Energy Budgets for Eastern Canadian and Northeast US Waters. *Continental Shelf Research* 30, 3–4, 353–64. https://doi.org/10.1016/j.csr.2009.12.003. 2010.

Bernier et al. : Regional Deterministic Storm Surge Prediction System (RDSPS) version 1.6.0. Technical Note, Canadian Meteorological Centre. Available at: https://collaboration.cmc.ec.gc.ca/cmc/CMOI/product_guide/docs/tech_notes/technote_rdsps-160_e.pdf, 2020.

Bobanović, J. : Barotropic Circulation Variability on Canadian Atlantic Shelves (Ph.D. thesis). Dalhousie University, Halifax, NS, Canada. 1997.

Bourgault, D. and Koutitonsky, V.G. : Real-time monitoring of the freshwater discharge at the head of the St. Lawrence Estuary. Atmosphere-Ocean, 37(2), pp.203-220, 1999.

Brasnett, B. : The impact of satellite retrievals in a global sea-surface temperature analysis. Quart. J. Roy. Meteor. Soc., 134, 1745– 1760, doi:10.1002/qj.319. 2008

Brasnett, B. and Surcel-Colan, D. : Assimilating Retrievals of Sea Surface Temperature from VIIRS and AMSR2, Journal of Atmospheric and Oceanic Technology, 33*(*2), 361-375. https://doi.org/10.1175/JTECH-D-15-0093.1, 2016.

Buehner, M., Caya, A., Pogson, L., Carrieres, T., and Pestieau, P.: A New Environment Canada Regional Ice Analysis System, Atmos. Ocean, 51(1), 18-34, 2013.

https://doi.org/10.5194/egusphere-2023-42
Preprint. Discussion started: 26 January 2023
© Author(s) 2023. CC BY 4.0 License.

Buehner, M., Caya, A., Carrieres, T. and Pogson, L.: Assimilation of SSMIS and ASCAT data and the replacement of highly uncertain estimates in the Environment Canada Regional Ice Prediction System. Q. J. Roy. Meteor. Soc., 142(695), 562-573, 2016.

Carrère L., Lyard, F., Cancet, M., Guillot, A. and Roblou, L.: FES2012: A new global tidal model taking taking advantage of nearly 20 years of altimetry, Proceedings of meeting "20 Years of Altimetry", Venice 2012.

Cirano, M., Charria, G., De Mey-Frémaux, P., Kourafalou, V. K. and Stanev, E.: Coastal Ocean Forecasting Science supported by GODAE OceanView Coastal Oceans and Shelf Seas Task Team (COSS-TT)—Part II Ocean Dynamics,https://doi.org/10.1007/s10236-021-01464-x.,2021.

Dai A., and Trenberth, K.E. : Estimates of freshwater discharge from continents: latitudinal and seasonal variations. Journal of hydrometeorology, 3, 660-687. 2002.

De Mey-Frémaux, P., Ayoub, N., Barth, A., Brewin, R., Charria, G., Campuzano, F., Ciavatta, S., Cirano, M., Edwards, C. A., Federico, I., Gao, S., Garcia Hermosa, I., Garcia Sotillo, M., Hewitt, H., Hole, L. R., Holt, J., King, R., Kourafalou, V., Lu, Y., Mourre, B., Pascual, A., Staneva, J., Stanev, E.V., Wang, H. and Zhu, X. : Model-Observations Synergy in the Coastal Ocean. Frontiers in Marine Science,6. doi:10.3389/fmars.2019.00436. 2019.

Dronkers, J. J. : Tidal computations for rivers, coastal areas, and seas. Journal of the hydraulics division, Proceedings of the American Society of Civil Engineers, 49. 1969.

Dupont, F., Higginson, S., Bourdallé-Badie, R., Lu, Y., Roy, F., Smith, G., Lemieux, J.F., Garric, G., and Davidson, F. : A high-resolution ocean and sea-ice modelling system for the Arctic and North Atlantic oceans. Geosci Model Dev 8(5):1577–1594. https://doi.org/10.5194/gmd-8-1577-2015. 2015

Dupont et al. : Water Cycle Prediction System (WCPS) version 3.0.0. Technical Note. Canadian Meteorological Center. https://collaboration.cmc.ec.gc.ca/cmc/CMOI/product_guide/docs/tech_notes/technote_wcps-300_e.pdf. 2021.

Durnford, D., Fortin, V., Smith, G. C., Archambault, B., Deacu, D., Dupont, F., Dyck, S., Martinez, Y., Klyszejko, E., MacKay, M., Liu, L., Pellerin, P., Pietroniro, A., Roy, F., Vu, V., Winter, B., Yu, W., Spence, C., Bruxer, J., and Dickhout, J. : Toward an Operational Water Cycle Prediction System for the Great Lakes and St. Lawrence River, Bulletin of the American Meteorological Society, 99(3), 521-546. 2018.

Egbert, G. D., and Erofeeva. S. Y. : Efficient inverse modeling of barotropic ocean tides. Journal of Atmospheric and Oceanic Technology 19.2. 183-204. 2002.

Flather, R.: A storm surge prediction model for the northern bay of bengal with application to the cyclone disaster in april 1991. J. Phys. Oceanogr., 24, 172–190. 1994

Foreman, M., Walters, R., Henry, R., Keller, C., and Dolling, A. : A tidal model for eastern Juan de Fuca Strait and the southern Strait of Georgia. Journal of Geophysical Research, 100(C1), 721–740. 1995.

Fringer, O. B., Dawson, C. N., He, R., Ralston, D. K., Zhang, Y. J. : The future of coastal and estuarine modeling: Findings from a workshop, Oc. Mod., Volume 143, https://doi.org/10.1016/j.ocemod.2019.101458. 2019.

https://doi.org/10.5194/egusphere-2023-42
Preprint. Discussion started: 26 January 2023
© Author(s) 2023. CC BY 4.0 License.

García Sotillo, M., Cailleau, S., Aznar, R., Aouf, L., Barrera, E., et al. : The Operational CMEMS IBI-MFC Service Today: Review of Major Achievements along the Copernicus-1 Service Phase (2015-2021). 9th EuroGOOS International conference, Shom; Ifremer; EuroGOOS AISBL, May 2021, Brest, France. pp.321-328. ffhal-03336265v2f. 2021.

595 Gasset, N., 2019. Global Deterministic Prediction System (GDPS), update from version 6.1.0 to version 7.0.0. 2021 https://collaboration.cmc.ec.gc.ca/cmc/cmoi/product_guide/docs/tech_specifications/tech_specifications_GDPS_e.pdf

Hirose, N., Usui, N., Sakamoto, K., Tsujino, H., Yamanaka, G., Nakano, H., Urakawa, S., Toyoda, T., Fujii, Y. and Kohna, N.: Development of a new operational system for monitoring and forecasting coastal and open-ocean states around Japan.

600 Ocean Dynamics **69**, 1333–1357. https://doi.org/10.1007/s10236-019-01306-x.2019.

Hunke, E.C. : Viscous-plastic sea ice dynamics with the EVP model: linearization issues, J. Comput. Phys., 170, 18–38. 2001.

Hunke, E. C., and Lipscomb, W. H.: CICE: The Los Alamos sea ice model. Documentation and software user's manual version 4.0 (Tech. Rep. LA-CC-06-012), Los Alamos, NM: Los Alamos National Laboratory, 2008.

Katavouta, A., Thompson, K.R., Lu, Y., Loder, J.W. :Interaction between the tidal and seasonal variability of the Gulf of

605 Maine and Scotian Shelf region. J Phys Oceanogr 46(11):3279–3298. https://doi.org/ 10.1175/JPO-D-15-0091.1. 2016.

Kourafalou, V.H., De Mey, P., Le Hénaff, M., Charria, G., Edwards, C.A., He, R., Herzfeld, M., Pascual, A., Stanev, E.V., Tintoré, J., Usui, N., van der Westhuysen, A.J., Wilkin, J. and Zhu, X.:Coastal Ocean Forecasting: system integration and evaluation. Journal of Operational Oceanography 8:sup1, pages s127-s146. 2015a.

Kourafalou, V.H., De Mey, P., Staneva, J., Ayoub, N. , Barth, A., Chao, Y., Cirano, M., Fiechter, J., Herzfeld, M., Kurapov,

610 A., Moore, A.M., Oddo, P., Pullen, J., van der Westhuysen, A. and Weisberg, R.H. : Coastal Ocean Forecasting: science foundation and user benefits, Journal of Operational Oceanography, 8:sup1, s147-167, DOI: 10.1080/1755876X.2015.1022348.2015b.

Koutitonsky, V. G., and Bugden, G. L.: The physical oceanography of the Gulf of St. Lawrence: A review with emphasis on the synoptic variability of the motion, in The Gulf of St. Lawrence: Small Ocean or Big Estuary?, edited by J.-C. Therriault,

615 Can. Spec. Publ. Fish. Aquat.Sci., 113, 57– 90. 1991.

Kurapov, A. L., Erofeeva, S. Y., and Myers, E.:. Coastal sea level variability in the US West Coast Ocean forecast system (WCOFS). Ocean Dynamics, 67(1), 23-36. doi: 10.1007/s10236-016-1013-4. 2017.

Large, W. G., and Yeager, S.: Diurnal to decadal global forcing for ocean and sea-ice models: The data sets and flux climatologies (No. NCAR/TN-460+STR). University Corporation for Atmospheric Research. doi:10.5065/D6KK98Q6

620 Lefaivre, D., A. D'Astous and P. Matte (2016): Hindcast of Water Level and Flow in the St. Lawrence River Over the 2005–2012 Period, Atmosphere-Ocean, DOI: 10.1080/07055900.2016.1168281. 2004.

Lemieux, J.-F., Beaudoin, C., Dupont, F., Roy, F., Smith, G.C., Shlyaeva, A., Buehner, M., Caya, A., Chen, J., Carrieres, T., Pogson, L., DeRepentigny, P., Plante, A., Pestieau, P., Pellerin, P., Ritchie, H., Garric, G. and Ferry, N.: The Regional Ice Prediction System (RIPS): verification of forecast sea ice concentration. Q.J.R. Meteorol. Soc, 142: 632-

625 643. https://doi.org/10.1002/qj.2526. 2016.

https://doi.org/10.5194/egusphere-2023-42
Preprint. Discussion started: 26 January 2023
© Author(s) 2023. CC BY 4.0 License.

Lemieux, J.-F., Tremblay, L. B., Dupont, F., Plante, M., Smith, G.C. and Dumont, D.: A basal stress parameterization for modeling landfast ice, J. Geophys. Res., 120(4), 3157-3173, doi: 10.1002/2014JC010678. 2015.

Lemieux, J.-F., Dupont, F., Blain, P., Roy, F., Smith, G.C. and Flato, G.M. : Improving the simulation of landfast ice by 815 combining tensile strength and a parameterization for grounded ridges, J. Geophys. Res., 121(10), 7354-7368. 2016b.

630 Levier, B., Treguier, A.-M., Madec, G. and Garnier, V.: Free surface and variable volume in the nemo code. Tech. rep., MERSEA MERSEA IP report WP09-CNRS-STR-03-1A, 47pp, available on the NEMO web site. 2007.

Lipscomb, W. H., Hunke, E.C., Maslowski, W., and Jakacki, J.: Ridging, strength, and stability in high-resolution sea ice models, J. Geophys. Res., 112 (C03S91), doi:10.1029/2005JC003355. 2007.

Lorente, P., Sotillo, M., Amo-Baladrón, A., Aznar, R., Levier, B., Sánchez-Garrido, J.C., Sammartino, S., de Pascual-Collar,

635 Á., Reffray, G., Toledano, C., and Álvarez-Fanjul, E.: Skill assessment of global, regional, and coastal circulation forecast models: Evaluating the benefits of dynamical downscaling in IBI (Iberia–Biscay–Ireland) surface waters. Ocean Science, 15, 967–996, doi:10.5194/os-15-967-2019. 2019b.

Madec, G., and Imbard, M.: A global ocean mesh to overcome the North Pole singularity. Clim. Dyn., 12, 381–388. 1996.

Madec G, et al.: NEMO ocean engine, Note du Pole de modélisation. France. Ver 3.6 stable, ISSN No 1288–1619. 2015.

640 Maraldi, C., Chanut, J., Levier, B., Ayoub, N.K., De Mey, P., Reffray, G., Lyard, F.H., Cailleau, S., Drévillon, M., Álvarez Fanjul, E., Sotillo, M.G. and Marsaleix, P.: NEMO on the shelf: assessment of the Iberia-Biscay-Ireland configuration. Ocean Science 9 (2013): 745-771. 2013.

Mellor, G., and Blumberg, A.: Wave Breaking and Ocean Surface Layer Thermal Response, Journal of Physical Oceanography, 34(3), 693-698. 2004.

645 Milbrandt, J.A., Bélair, S., Faucher, M., Vallée, M., Carrera, M.L. and Glazer, A.: The pan-Canadian high resolution (2.5 km) deterministic prediction system. Weather Forecast 31(6):1791–1816. https://doi.org/10.1175/WAF-D-16-0035.1. 2016.

Nudds, S., Lu, Y., Higginson, S., Haigh, S.P., Paquin, J.-P., O'Flaherty-Sproul, M., Taylor, S., Blanken, H., Marcotte, G., Smith, G.C., Bernier, N.B., MacAulay, P., Wu, Y., Zhai, L., Hu, X., Chanut, J., Dunphy, M., Dupont, F., Greenberg, D., Davidson, F.J.M., Page, F.: Evaluation of Structured and Unstructured Models for Application in Operational Ocean

650 Forecasting in Nearshore Waters. Journal of Marine Science and Engineering. 8(7):484. https://doi.org/10.3390/jmse8070484. 2020

Paquin, J.-P., Lu, Y., Taylor, S., Blanken, H., Marcotte, G., Hu, X., Zhai, L., Higginson, S., Nudds, S., Chanut, J., Smith, G.C., Bernier, N. and Dupont, F.: High-resolution modelling of a coastal harbour in the presence of strong tides and significant river runoff. Ocean Dynamics **70,** 365–385. https://doi.org/10.1007/s10236-019-01334-7. 2020.

655 Paquin, J.-P., Roy, F., Smith, G.C., Dupont, F., MacDermid, S., Hata, Y., Huizy, O., Lei, J., Lu, Y., Taylor, S., Blanken, H.:. Coastal Ice Ocean Prediction System for the East Coast of Canada (CIOPS-E) – System description for version 1. *Canadian Centre for Meteorological and Environmental Prediction Technical Note*. April 20th 2022. [available at: Index of /cmc/CMOI/product_guide/docs/tech_notes]. 2022

https://doi.org/10.5194/egusphere-2023-42
Preprint. Discussion started: 26 January 2023
© Author(s) 2023. CC BY 4.0 License.

Paquin, J.-P., Roy, F., Smith, G.C., Dupont, F., MacDermid, S., Hata, Y., Huizy, O., Lei, J., Martinez, Y., Blanken, H., Holden, J., Soontiens, N.: Coastal Ice Ocean Prediction System for the East Coast of Canada (CIOPS-E) – Update from version 1.5.0 to 2.0.0. *Canadian Centre for Meteorological and Environmental Prediction Technical Note.* December 1st 2021. [available at: Index of /cmc/CMOI/product_guide/docs/tech_notes]. 2022

Pawlowicz, R., Beardsley, B., and Lentz, S.: Classical tidal harmonic analysis including error estimates in MATLAB using T TIDE. Computers & Geosciences, 28(8), 929–937. 2002.

Pellerin, P., Ritchie, H., Saucier, F. J., Roy, F., Desjardins, S., Valin, M., and Lee, V. : Impact of a Two-Way Coupling between an Atmospheric and an Ocean-Ice Model over the Gulf of St. Lawrence, Monthly Weather Review, 132(6), 1379-1398. 2004.

Rascle, N., Ardhuin, F., Queffeulou, P., and Croizé-Fillon, D. : A global wave parameter database for geophysical applications. Part 1: Wave-current–turbulence interaction parameters for the open ocean based on traditional parameterizations. Ocean Modelling, **25**, Issues 3–4, p. 154-171, https://doi.org/10.1016/j.ocemod.2008.07.006. 2008.

Reszka, M.K. and Swaters, G.E.:, 1999. Numerical investigation of baroclinic instability in the Gaspé Current using a frontal geostrophic model. Journal of Geophysical Research: Oceans, 104(C11), pp.25685-25696.

Roy, F., Bélanger, J.-M., Dyck, S., Dupont, F., J.-F. Lemieux, Beaudoin, C., Chanut, J., Garric, G., Pellerin, P. Ritchie, H., Lu, Y., and Davidson, F. : Update of the Regional Marine Prediction System – Gulf of St. Lawrence (RMPS-GLS) with NEMO-CICE. . *Canadian Centre for Meteorological and Environmental Prediction Technical Note.* December 1st 2021. [available at: https://collaboration.cmc.ec.gc.ca/cmc/cmoi/product_guide/docs/lib/technote_rmps-gsl-600_20141118_e.pdf]. 2014.

Roy, F., Chevallier, M., Smith, G. C., Dupont, F., Garric, G., Lemieux, J.-F., Lu, Y. and Davidson, F. 2015. Arctic sea ice and freshwater sensitivity to the treatment of the atmosphere-ice-ocean surface layer. J. Geophys. Res. - Oceans, 120(6), 4392-880 4417. 2015.

Sakamoto, K., Tsujino, H., Nakano, H., Urakawa, S., Toyoda, T.Hirose, N., Usui, N., and Yamanaka, G. : Development of a 2-km resolution ocean model covering the coastal seas around Japan for operational application. Ocean Dynamics 69, 1181–1202. https://doi.org/10.1007/s10236-019-01291-1. 2019.

Saucier, F.J. and Chassé, J.: Tidal circulation and buoyancy effects in the St. Lawrence Estuary. Atmosphere-Ocean, 38(4), pp.505-556. 2000.

Saucier, F. J., Roy, F., Gilbert, D., Pellerin, P., and Ritchie, H. : Modeling the formation and circulation processes of water masses and sea ice in the Gulf of St. Lawrence, Canada, *J. Geophys. Res.*, 108, 3269, doi:10.1029/2000JC000686, C8. 2003

Shchepetkin, A. F., and J. C. McWilliams : The regional oceanic modeling system (roms) - a split-explicit, free-surface, topography-following-coordinate oceanic modelr. Ocean Modelling, 9 (4), 347–404. 2005

Sheng, J. : Dynamics of a Buoyancy-Driven Coastal Jet: The Gaspé Curreny, *Journal of Physical Oceanography* 31, 11: 3146-3162. https://doi.org/10.1175/1520-0485(2001)031<3146:DOABDC>2.0.CO;2. 2001

Smagorinsky, J., : Large Eddy Simulation of Complex Engineering and Geophysical Flows, chap. Some historical remarks on the use of non-linear viscosities, 3–36. Cambridge University Press, B. Galperin and S. A. Orszag (eds.). 1993.

https://doi.org/10.5194/egusphere-2023-42
Preprint. Discussion started: 26 January 2023
© Author(s) 2023. CC BY 4.0 License.

Smith, S.D., Anderson, R.J., Oost, W.A. Kraan,C., Katsaros, K.B., Davidson, K. L., Bumke, K., Hasse, L., and Chadwick, H.M.: Sea surface wind stress and drag coefficients: The hexos results. Boundary-Layer Meteorol 60, 109–142. https://doi.org/10.1007/BF00122064. 1992.

Smith, G. C., Saucier, F. J. , and Straub, D.: Formation and circulation of the cold intermediate layer in the Gulf of Saint Lawrence, J. Geophys. Res., 111, C06011, doi:10.1029/2005JC003017. 2006a.

Smith, G. C., Saucier, F. J., and Straub D. : Response of the lower St. Lawrence estuary to external forcing in winter, J. Phys. Oceanogr., 36(8), 1485-1501. doi: 10.1175/JPO2927.1. 2006b.

Smith, G.C., Roy, F. and Brasnett, B.: Evaluation of an operational ice–ocean analysis and forecasting system for the Gulf of St Lawrence. Quarterly Journal of the Royal Meteorological Society, 139(671), pp.419-433. 2013.

Smith, G. C., Roy, F., Reszka, M., Surcel Colan, D., He, Z., Deacu, D., Belanger, J. M., Skachko, S., Liu, Y., Dupont, F. and Lemieux, J.-F.: Sea ice forecast verification in the Canadian global ice ocean prediction system, Q. J. Roy. Meteor. Soc., 142(695), 659-671, doi: 10.1002/qj.2555. 2016.

Smith, G.C., Liu, Y., Benkiran, M., Chikhar, K., Surcel Colan, D., Gauthier, A.A., Testut, C.E., Dupont, F., Lei, J., Roy, F. and Lemieux, J.F.: The Regional Ice Ocean Prediction System v2: a pan-Canadian ocean analysis system using an online tidal harmonic analysis. Geoscientific Model Development, 14(3), pp.1445-1467. 2021.

Thompson, K.R., Sheng, J.Y., Smith, P.C., and Cong, L.Z.: Prediction of surface currents and drifter trajectories on the inner Scotian shelf. Journal of Geophysical Research-Oceans 108, 3287doi:10.1029/2001JC001119. 2003.

Thompson, K. R., Wright, D. G., Lu, Y., and Demirov, E.: A simple method for reducing seasonal bias and drift in eddy resolving ocean models, Ocean Modell., 13(2), 109– 125. 2006.

Tonani, M., Sykes, P., King, R. R., McConnell, N., Péquignet, A.-C., O'Dea, E., Graham, J. A., Polton, J., and Siddorn, J.: The impact of a new high-resolution ocean model on the Met Office North-West European Shelf forecasting system, Ocean Sci., 15, 1133–1158, https://doi.org/10.5194/os-15-1133-2019, 2019.

Trotta, F., Fenu, E., Pinardi, N., Bruciaferri, D., Giacomelli, L., Federico, I., Gi, C.: A structured and unstructured grid relocatable ocean platform for forecasting (SURF). Deep Sea Res II Top Stud Oceanogr. 133:54–75. 2016.

Trotta, F., Pinardi, N., Fenu, E., Grandi, A., and Lyubartsev, V.: Multi-nest high-resolution model of submesoscale circulation features in the Gulf of Taranto. Ocean Dyn 67(12):1609–1625. https://doi.org/10.1007/s10236-017-1110-z. 2017.

Umlauf, L., and Burchard, H. : A generic length-scale equation for geophysical turbulence models. Journal of Marine Research, 61(2), 235–265. 2003.

https://doi.org/10.5194/egusphere-2023-42
Preprint. Discussion started: 26 January 2023
© Author(s) 2023. CC BY 4.0 License.

Table 1: Main ocean model parameters

Parameter	RIOPS v2.0	CIOPS-E
NEMO version	3.6	3.6
Time step	300s (barotropic 5s)	150s (barotropic 5s)
Vertical levels	75	100
Momentum advection	3rd order ubs	3rd order ubs
BDY Barotropic	Flather	Flather
BDY Baroclinic dyn	Specified	Specified
BDY tracer	Specified	Specified
Lateral diff. momentum	Lap. (50m2/s)	Bilaplacian + smagorinski
Lateral mom. cond.	Free slip	Partial slip (shlat=1.0)
Lateral diff. tracers	Bilap.	Laplacian + smagorinski
Bottom friction	Non-linear / loglayer	Non-linear / loglayer
Vertical diffusion	k-ε (GLS)	k-ε (GLS)
Solar penetration	2-band	2-band
Large-scale "correction"	Data assimilation	Spectral nudging
Ocean boundary data	GIOPS	RIOPS-F
Tides	OSU / FES (13)	OSU / FES (13)
Atmospheric forcing	Blended GDPS – RDPS	Blended GDPS – HRDPS
Atm. forcing resolution	25 km – 10 km	25 km – 2.5 km
Forcing frequency	3h	1h
Atmospheric pressure	Yes	Yes
River runoff*	Dai&Trenberth +1d St Laurent	Dai&Trenberth, Saucier et al. (2003) & 1d St Laurent

https://doi.org/10.5194/egusphere-2023-42
Preprint. Discussion started: 26 January 2023
© Author(s) 2023. CC BY 4.0 License.

Table 2: Statistics for daily-averaged residual time series (see fig.1 for stations locations)

No		RMSE			CORR			GAMMA		
	Tide Gauge	CIOPS-E	RIOPS	RMPS-GSL	CIOPS-E	RIOPS	RMPS-GSL	CIOPS-E	RIOPS	RMPS-GSL
1	St-François-de-l'Île-d'Orléans	0.097		0.112	0.90		0.87	0.21		0.28
2	St-Joseph-de-la-Rive	0.053	0.132	0.104	0.95	0.71	0.79	0.10	0.62	0.39
3	Rimouski	0.043	0.060	0.093	0.93	0.89	0.57	0.14	0.28	0.67
4	Sept-Îles	0.030	0.045	0.089	0.97	0.94	0.69	0.06	0.14	0.53
5	Rivière-au-Renard	0.048	0.060	0.093	0.88	0.84	0.36	0.26	0.40	0.98
6	Belledune	0.035	0.047	0.091	0.95	0.92	0.64	0.09	0.16	0.59
7	Lower-Escuminac	0.041	0.044	0.094	0.94	0.94	0.64	0.11	0.13	0.59
8	Shediac Bay	0.045	0.061	0.095	0.95	0.91	0.76	0.09	0.17	0.42
9	Charlottetown	0.046	0.061	0.100	0.92	0.86	0.52	0.15	0.27	0.72
10	Cap-aux-Meules	0.040	0.061	0.095	0.92	0.83	0.47	0.15	0.34	0.85
11	Port-aux-Basques	0.036	0.045	0.095	0.93	0.89	0.28	0.13	0.21	0.93
12	St-Lawrence	0.037	0.046		0.95	0.91		0.11	0.17	
13	Argentia	0.040	0.051		0.94	0.90		0.11	0.19	
14	St John	0.039	0.055		0.97	0.93		0.07	0.14	
15	Bonavista	0.035	0.054		0.97	0.93		0.07	0.15	
16	North Sydney	0.031	0.055	0.091	0.96	0.87	0.59	0.08	0.25	0.66
17	Halifax	0.036	0.053		0.95	0.87		0.11	0.24	
18	Yarmouth	0.039	0.049		0.93	0.88		0.15	0.23	
19	St John	0.051	0.069		0.87	0.75		0.25	0.48	
20	Eastport	0.043	0.060		0.91	0.81		0.22	0.44	
21	Bar Harbor	0.031	0.041		0.96	0.93		0.10	0.17	
22	Wells	0.032	0.042		0.97	0.94		0.08	0.13	
23	Boston	0.033	0.037		0.97	0.95		0.08	0.10	
24	Woods Hole	0.029	0.044		0.97	0.93		0.06	0.14	
25	Montauk	0.028	0.043		0.98	0.95		0.05	0.11	
26	Sandy Hook	0.035	0.041		0.98	0.97		0.05	0.07	
27	Atlantic City	0.039	0.050		0.97	0.95		0.06	0.09	
28	Lewes	0.036	0.048		0.98	0.96		0.05	0.08	
29	Duck	0.043	0.052		0.96	0.94		0.07	0.11	

https://doi.org/10.5194/egusphere-2023-42
Preprint. Discussion started: 26 January 2023
© Author(s) 2023. CC BY 4.0 License.

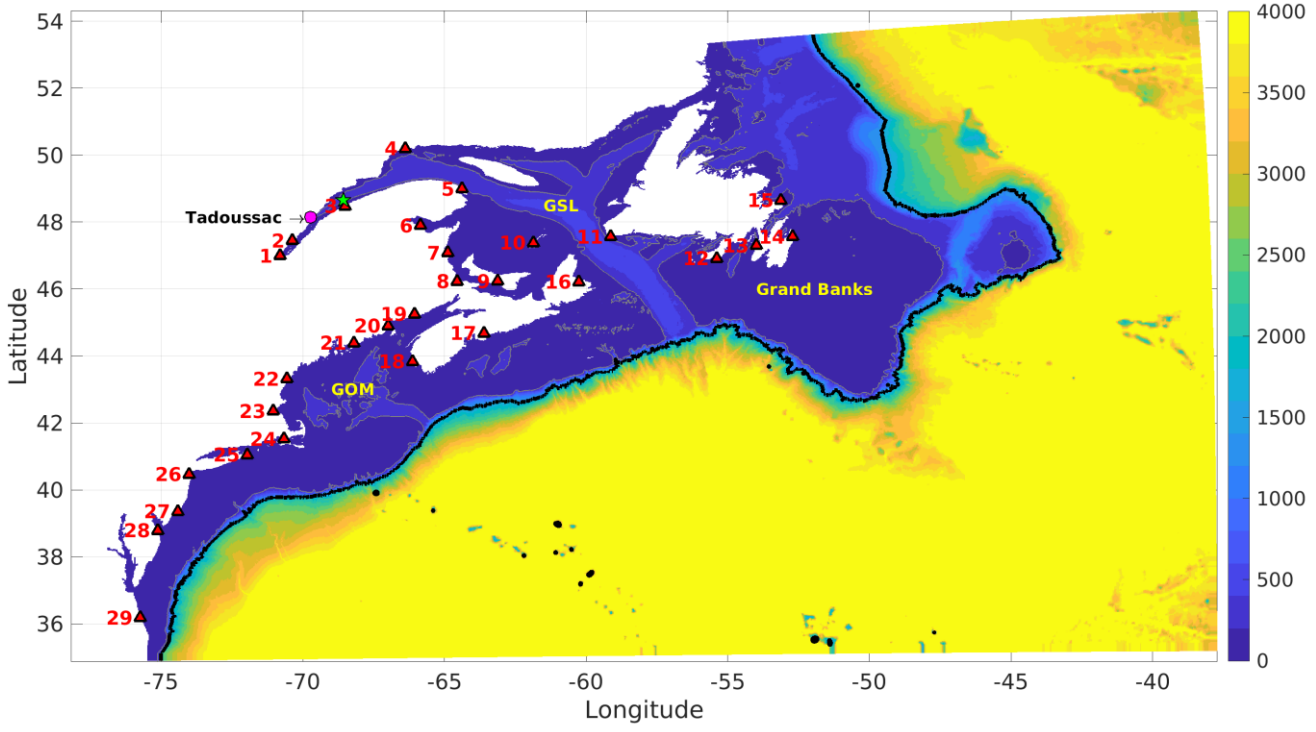

730 **Figure 1: Bathymetry (m, colors) over the NWA36 domain used by CIOPS-E. The grey and black lines show the 200m and 1500m isobaths, respectively. Red triangles shows the coastal tide gauges referenced in the text and in Table 2. The location of IML-4 buoy and Tadoussac are identified by the green star and magenta circle respectively. The Gulf of Maine and the Gulf of St. Lawrence area are identified by GOM and GSL respectively.**

https://doi.org/10.5194/egusphere-2023-42
Preprint. Discussion started: 26 January 2023
© Author(s) 2023. CC BY 4.0 License.

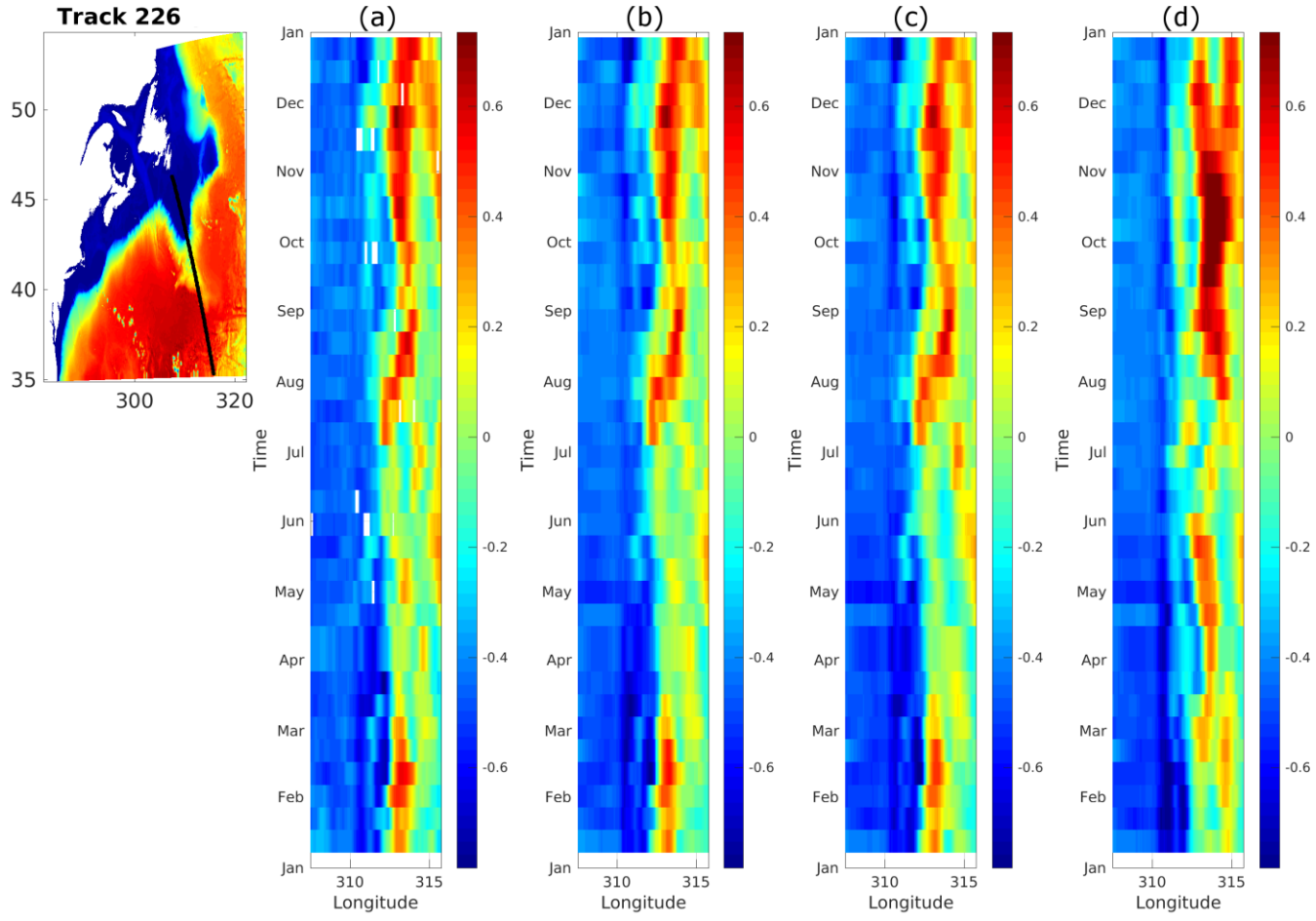

Figure 2: Along-track sea surface anomaly comparison for a Jason 2 altimetry track (#226). The left panel shows CIOPS-E bathymetry (colour) and the track position (black line). The four subsequent panels show Hovmöller diagrams along the track longitude for each altimeter swath on a 10-days recurring period for (a) altimeter data (b) RIOPS, (c) spectral nudging and (d) free run of CIOPS-E, respectively.

https://doi.org/10.5194/egusphere-2023-42
Preprint. Discussion started: 26 January 2023
© Author(s) 2023. CC BY 4.0 License.

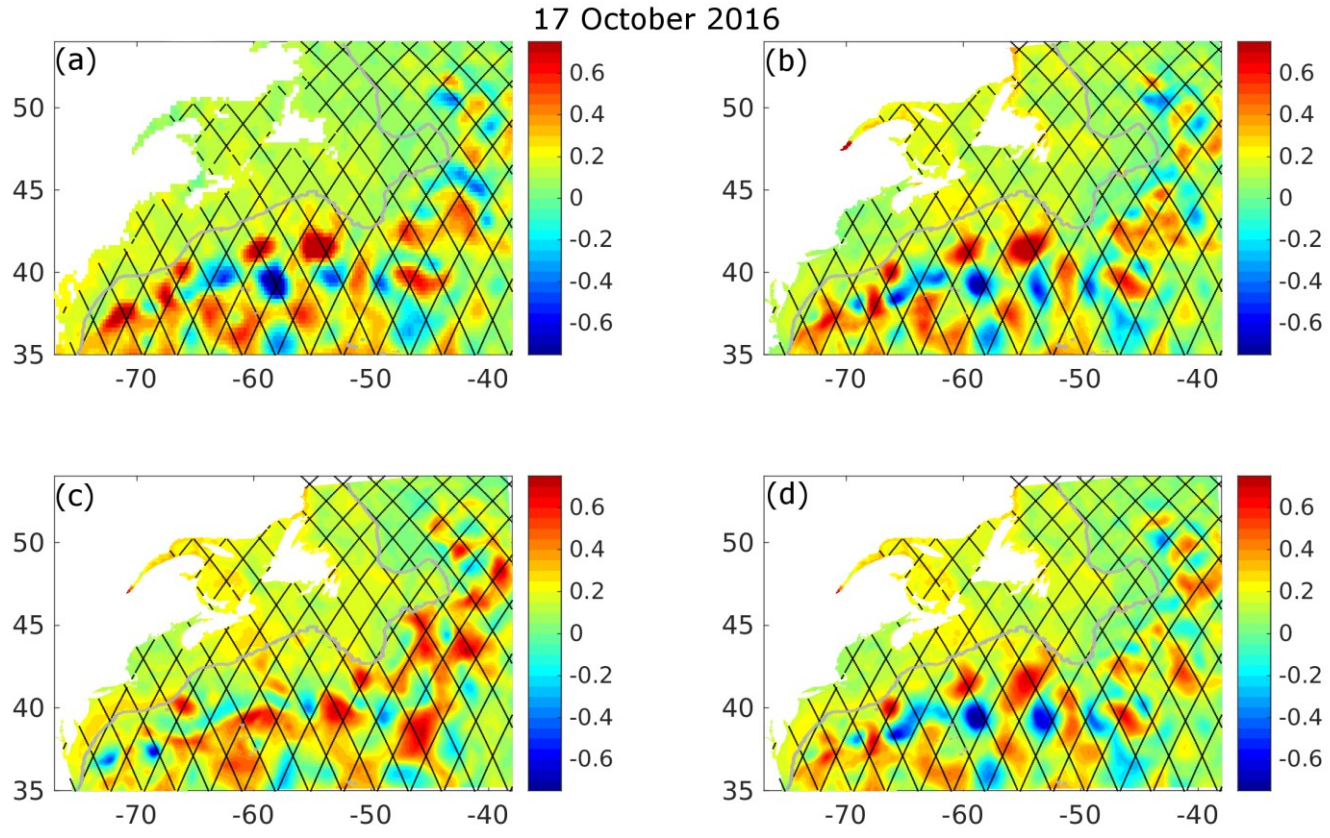

Figure 3: Comparison of Sea level anomaly on October 17th, 2016 for (a) gridded altimetry product, (b) RIOPS, (c) CIOPS-E "free-run" simulation and (d) CIOPS-E simulation constrained with spectral nudging. The thick grey lines on each panel represent the 1500 m isobaths. Thin black lines represent altimeter tracks over the model domain

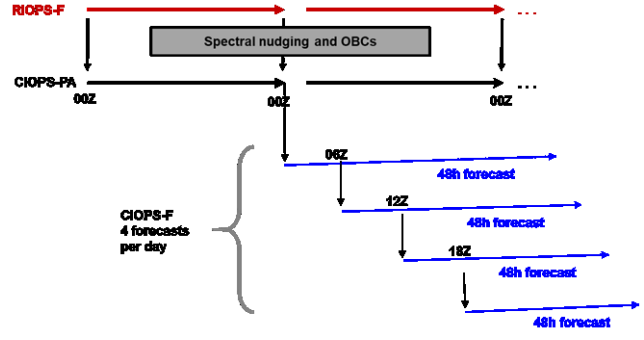

Figure 4: Schematic of CIOPS-E execution. The CIOPS pseudo-analysis (CIOPS-PA) is executed each day for a 24h period, restarting from its previous execution as initial conditions. The forecast component of RIOPS provides boundary conditions and large-scale fields for spectral nudging to the PA. CIOPS-E forecast performs four 48h forecast per day at 00Z, 06Z, 12Z & 18Z using initial conditions from the PA for the 00Z or a restart file at hour 06 from the previous forecast for 06Z, 12Z and 18Z

https://doi.org/10.5194/egusphere-2023-42
Preprint. Discussion started: 26 January 2023
© Author(s) 2023. CC BY 4.0 License.

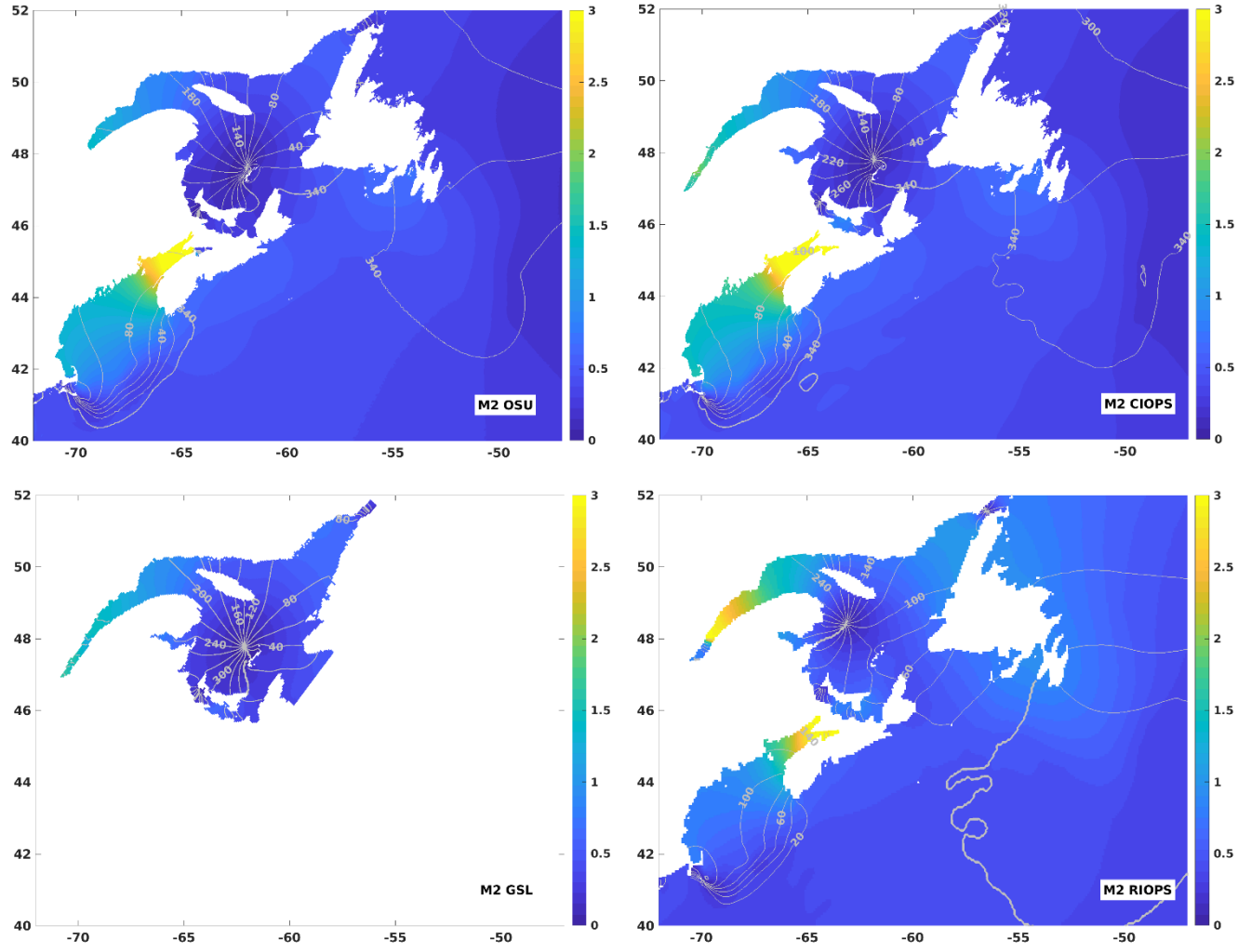

Figure 5 : Comparison of co-amplitude (colors) and co-phase (lines) for the principal lunar semidiurnal (M2) tidal constituent between Oregon State University (OSU, top left), CIOPS-E (top right), RMPS-GSL (bottom left) and RIOPS (bottom right).

https://doi.org/10.5194/egusphere-2023-42
Preprint. Discussion started: 26 January 2023
© Author(s) 2023. CC BY 4.0 License.

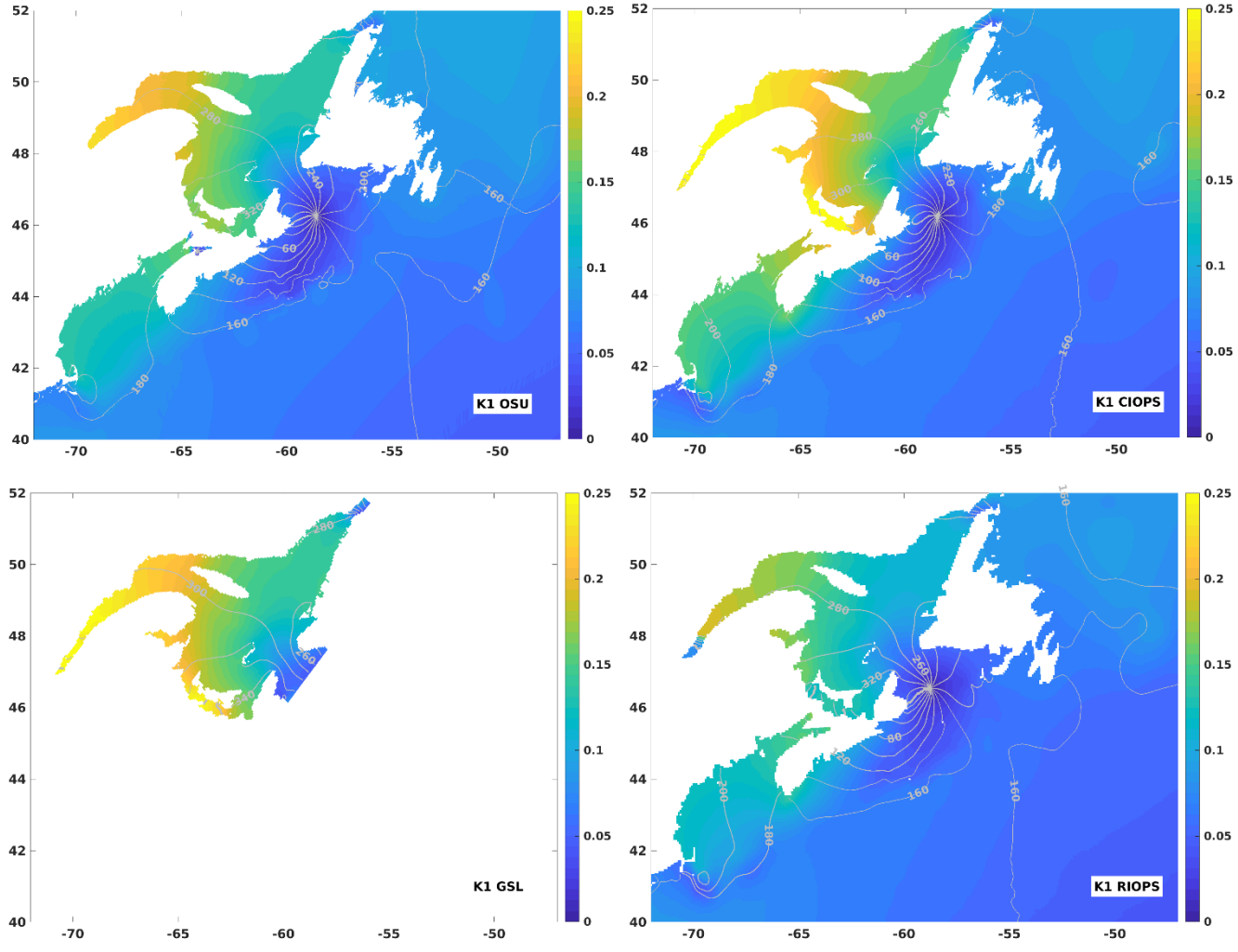

Figure 6 : Comparison of co-amplitude (colors) and co-phase (lines) for the lunar diurnal (K1) tidal constituent between Oregon State University (OSU, top left), CIOPS-E (top right), RMPS-GSL (bottom left) and RIOPS (bottom right).

https://doi.org/10.5194/egusphere-2023-42
Preprint. Discussion started: 26 January 2023
© Author(s) 2023. CC BY 4.0 License.

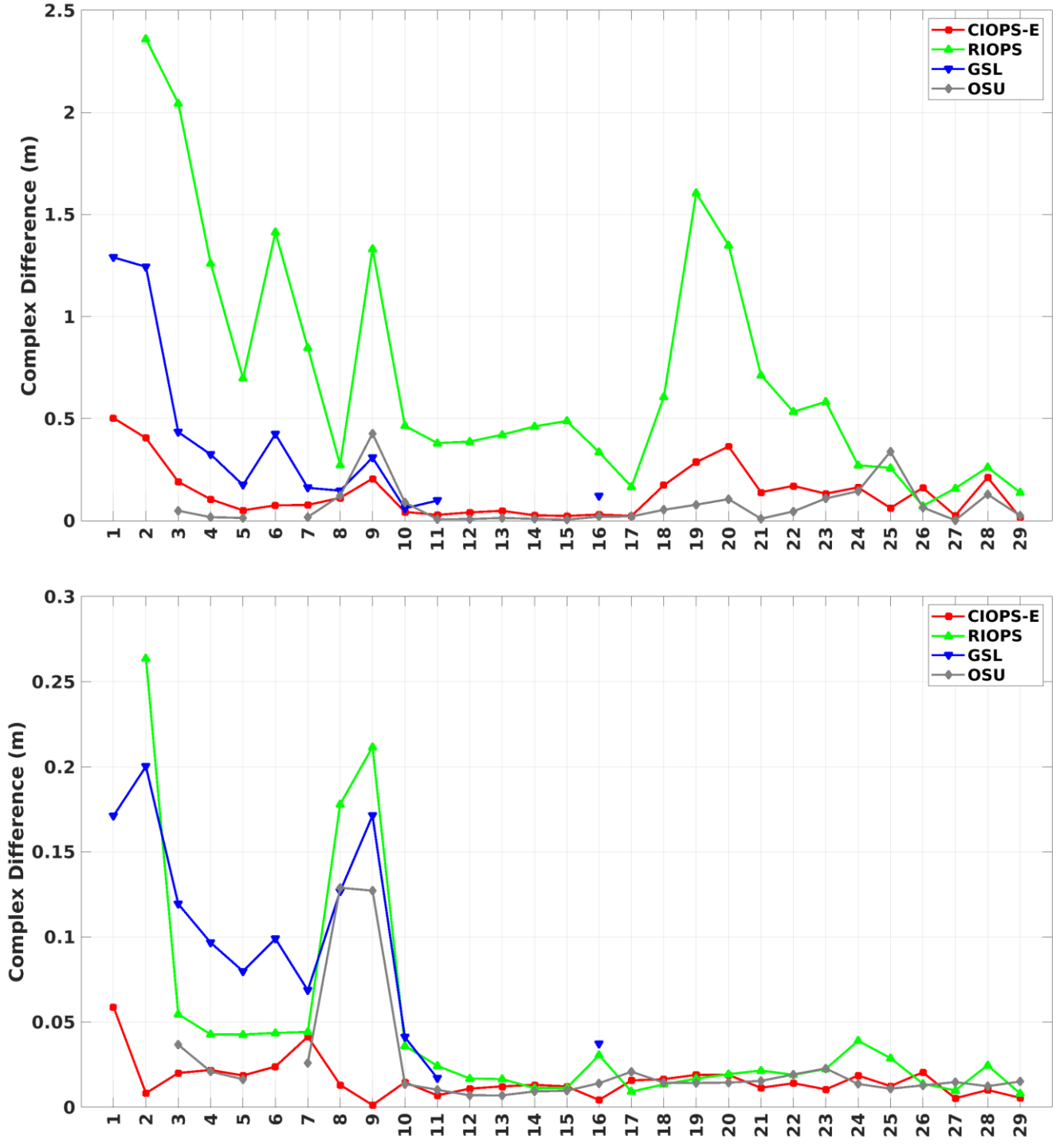

Figure 7: Complex differences (m) calculated at coastal tide gauges for M2 (top) and K1 (bottom) tidal constituents for CIOPS-E (red), RIOPS (green), RMPS-GSL (blue) and OSU (gray). Stations are numbered according to Fig.1 and organized from the St. Lawrence Estuary towards the GSL, Newfoundland, Bay of Fundy – Gulf of Maine, ending with the East Coast of the United States.

https://doi.org/10.5194/egusphere-2023-42
Preprint. Discussion started: 26 January 2023
© Author(s) 2023. CC BY 4.0 License.

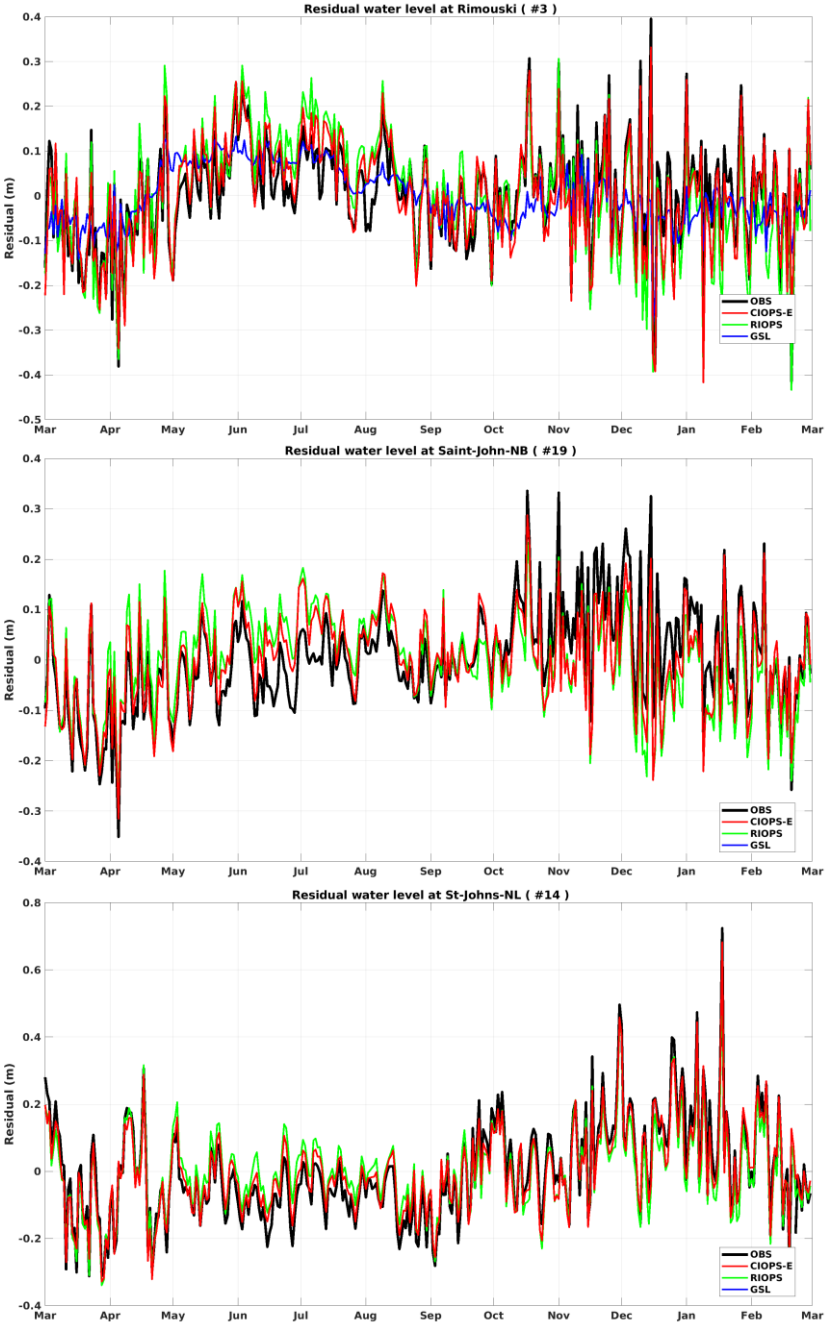

Figure 8: Daily-averaged residual water levels at the Rimouski (top), St John NB (middle) and St John's NL (bottom) coastal tide gauges for observations (black), CIOPS-E (red), RIOPS (green) and RMPS-GSL (blue) from March 1st 2019 to February 29th 2020.

https://doi.org/10.5194/egusphere-2023-42
Preprint. Discussion started: 26 January 2023
© Author(s) 2023. CC BY 4.0 License.

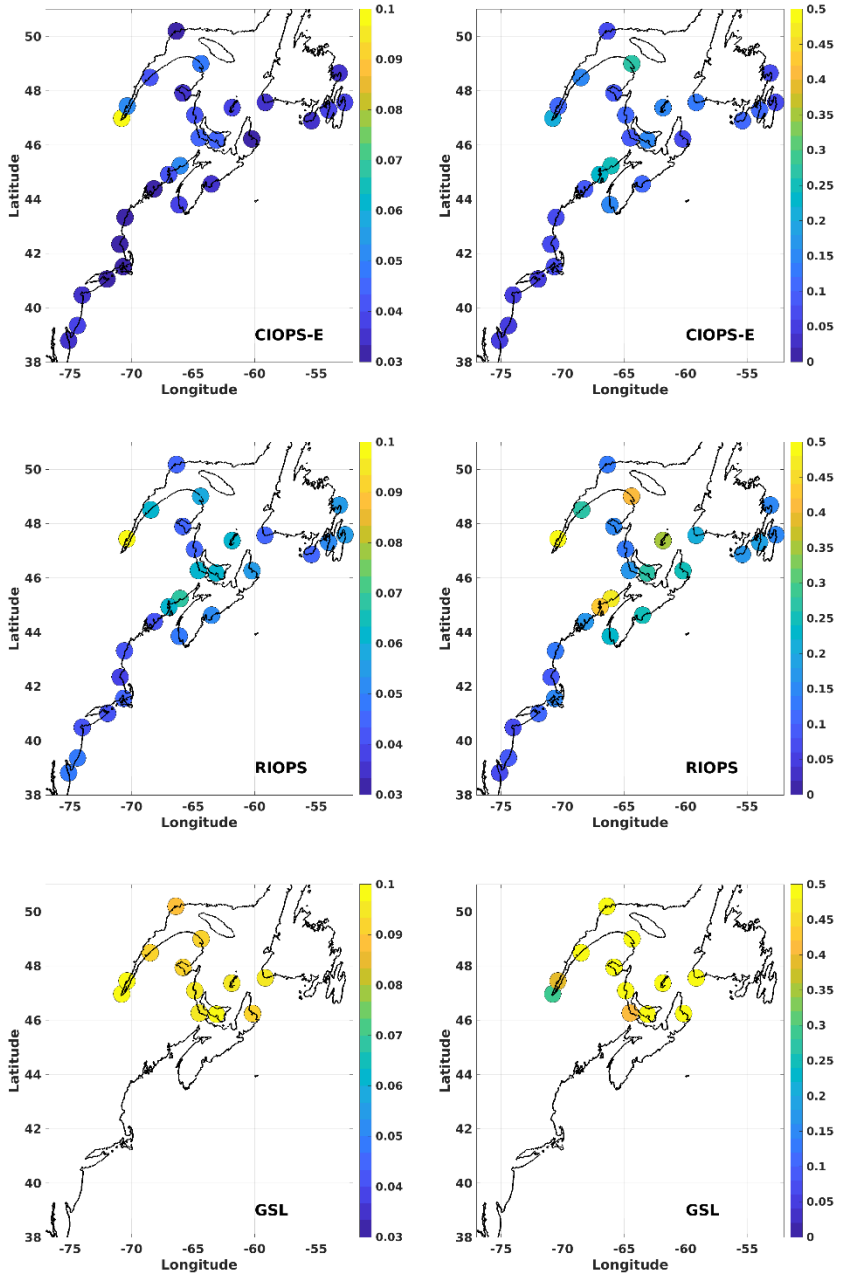

760

Figure 9: Root-mean-square errors (left) and gamma-square score (right) for daily averaged sub-tidal water levels at coastal tide gauges for CIOPS-E (top), RIOPS (center) and RMPS-GSL (bottom). Note the difference in colour bars between the two columns.

https://doi.org/10.5194/egusphere-2023-42
Preprint. Discussion started: 26 January 2023
© Author(s) 2023. CC BY 4.0 License.

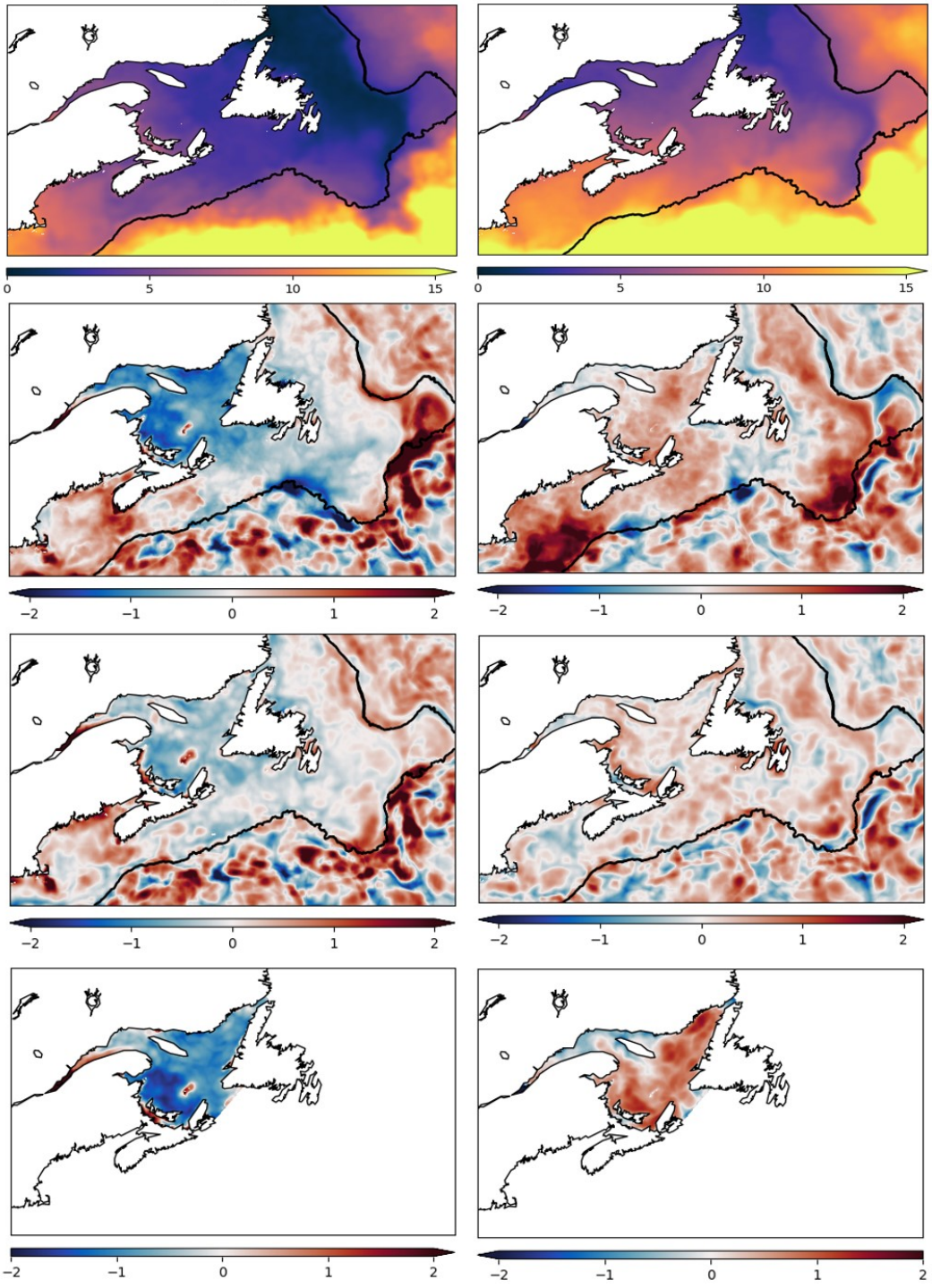

Figure 10: (1st row) CCMEP SST Analysis for (left) April to June 2019 and (right) October to December. Difference with CIOPS-E (2nd row), RIOPS (3rd row) and RMPS-GSL (4th row), respectively.

https://doi.org/10.5194/egusphere-2023-42
Preprint. Discussion started: 26 January 2023
© Author(s) 2023. CC BY 4.0 License.

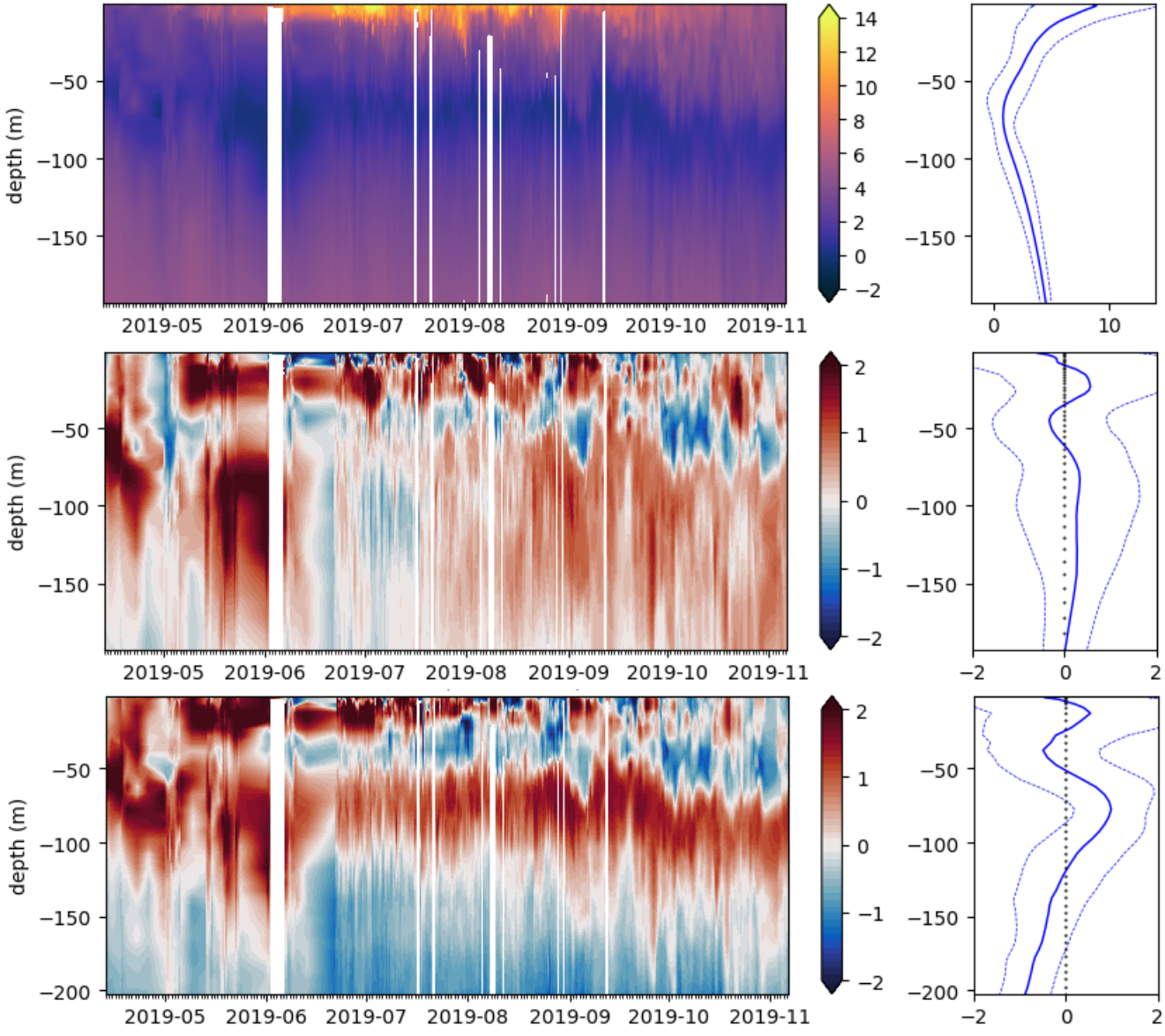

Figure 11 : Evolution of (top) the observed temperature profiles (OBS) at IML-4 station in the St. Lawrence Estuary (see location on Fig.1), from April to mid-November 2019, along with temperature differences from CIOPS-E minus OBS (middle) and RMPS-GSL minus OBS (bottom) models. Right panels show the time-averaged profiles of the Hovmoller plots as thick lines with dashed lines representing the plus or minus one standard deviation.

https://doi.org/10.5194/egusphere-2023-42
Preprint. Discussion started: 26 January 2023
© Author(s) 2023. CC BY 4.0 License.

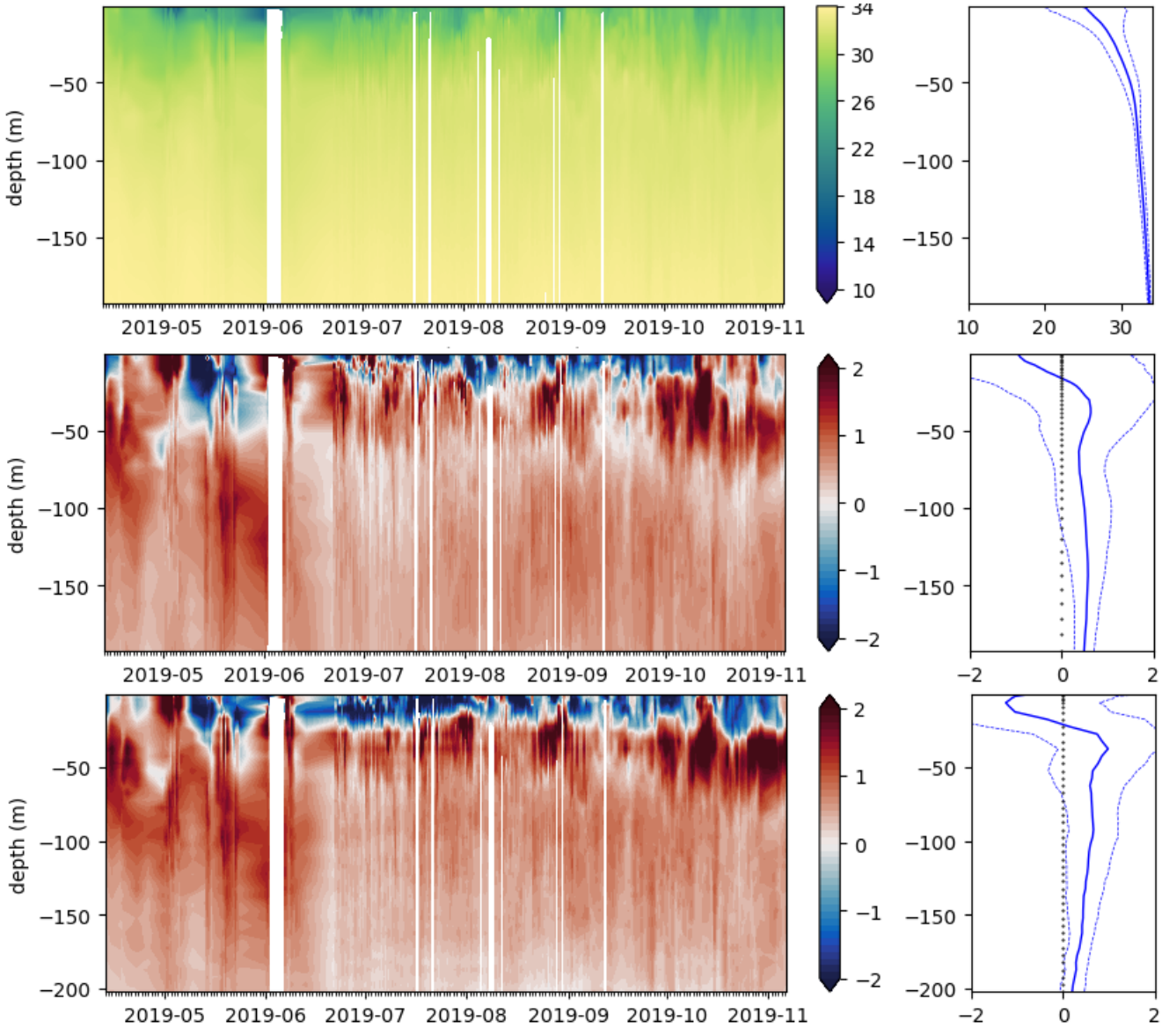

Figure 12: Same as Figure 11 but for salinity (PSU).

https://doi.org/10.5194/egusphere-2023-42
Preprint. Discussion started: 26 January 2023
© Author(s) 2023. CC BY 4.0 License.

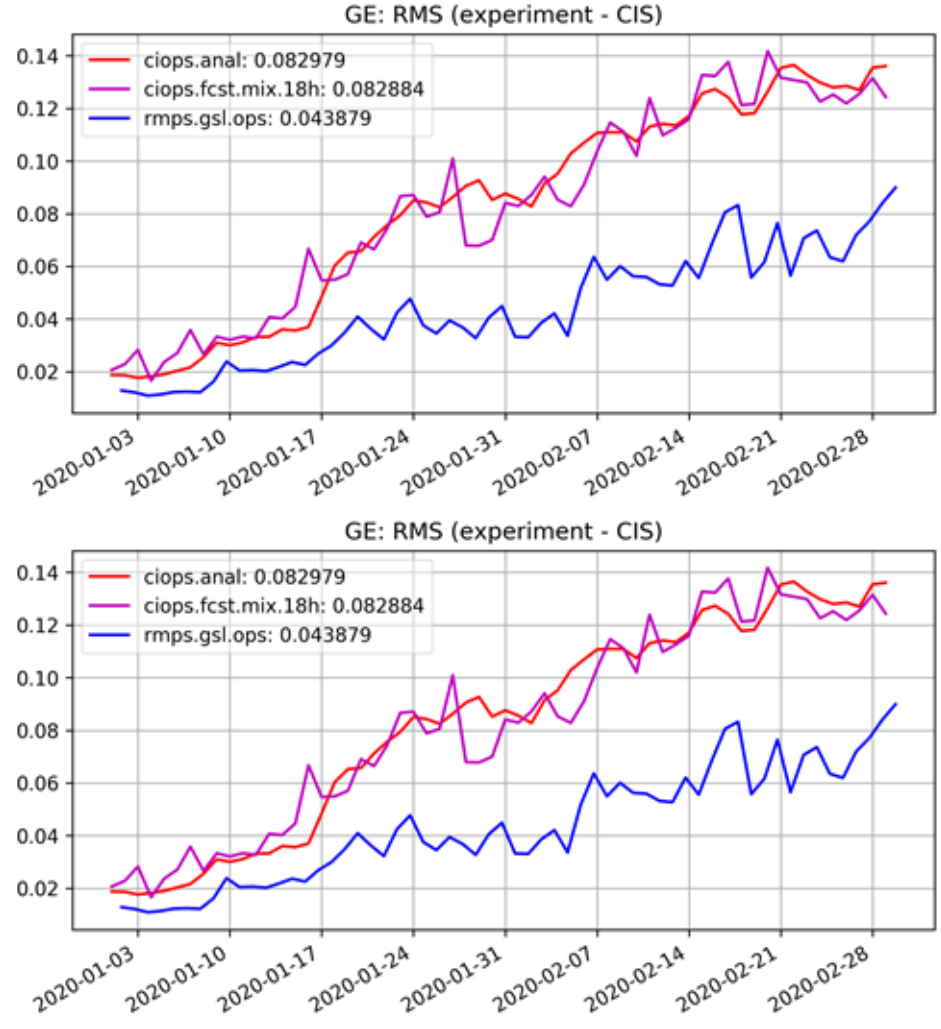

Figure 13: Evolution of the sea ice cover RMS error relative to RadarSat2 images analysed by CIS (GL: top) and thickness (GE: bottom) over the winter of 2020 in CIOPS-E pseudo-analysis (red), the CIOPS-E forecasts (purple) and the operational RMPS-GSL (blue).

https://doi.org/10.5194/egusphere-2023-42
Preprint. Discussion started: 26 January 2023
© Author(s) 2023. CC BY 4.0 License.

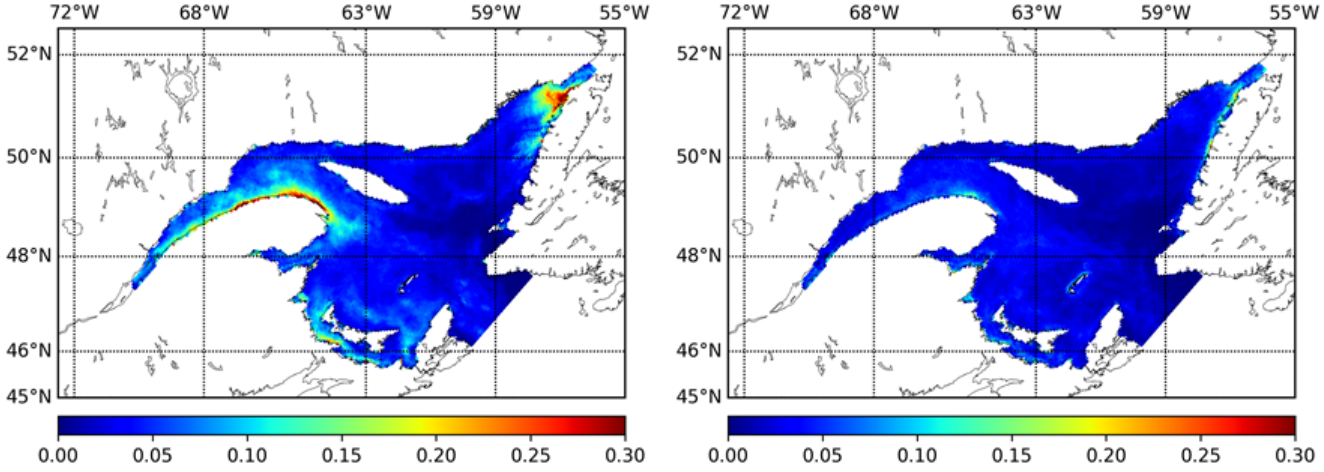

Figure 14: Mean Absolute Error (in m) of the sea ice thickness compared to Radarsat "stage of development" estimates for CIOPS-E (left) and the RMPS-GSL (right).